LITHOS 454-455 (2023) 107239

Contents lists available at ScienceDirect

LITHOS

journal homepage: www.elsevier.com/locate/lithos

Meso-Neoproterozoic basic-intermediate mafic granulites (metabasites) from the ~1 Ga granulitic southwestern Oaxacan complex, Mexico, crustal evolution and phase equilibria modeling

Laura Culí [a,b,*], Joan Reche [a], Jesús Solé [b,c], Fernando Ortega-Gutiérrez [b]

[a] Departament de Geologia, Universitat Autònoma de Barcelona, 08193 Cerdanyola del Vallès, Spain
[b] Universidad Nacional Autónoma de México, Instituto de Geología, Cd. Universitaria, 04510 Ciudad de México, Mexico
[c] Laboratorio Nacional de Geoquímica y Mineralogía (LANGEM), Cd. Universitaria, 04510 Ciudad de México, Mexico

ARTICLE INFO

Keywords:
Island/magmatic arc
Grenvillian orogen
Southwestern Oaxacan complex
Metabasite geochemistry
Restite
Partial melting

ABSTRACT

The basement of eastern Mexico is made up of Grenvillian granulite-facies metamorphic rocks, which constitute an inferred microcontinent named Oaxaquia. Proto-Oaxaquia oceanic arc reconstructions are related to the transition from Columbia to Rodinia supercontinents (~1.5 Ga). This study focuses on the petrography, geochemistry, and phase equilibria modeling of metabasites from the southwestern Oaxacan Complex, the largest Oaxaquia outcrop. Southwestern Oaxacan Complex protoliths mainly correspond to gabbro/basalt. They constitute an assemblage apart from the rest of the Oaxacan Complex metabasites due to their Ti enrichment and SiO_2 depletion related to post-magmatic/metamorphic processes. Southern study site metabasites correspond to the primitive root of the arc, mostly related to a divergent geotectonic setting. The other metabasites are related to the magmatic back/forearc active margin between proto-Oaxaquia and Amazonia craton. Phase equilibria modeling point to Zapotecan (last Grenvillian cycle) metamorphic peak conditions of 850 ± 25 °C and 1.0 ± 0.15 GPa from one garnet-amphibole bearing metabasite, and a later hydration episode (post-Grenvillian) of 760 ± 10 °C and 0.8 ± 0.20 GPa derived from one amphibole bearing metabasite. The time of incipient partial melting of the southwestern Oaxacan Complex is a pre-Zapotecan event (~1 Ga). Mineral textures do not display significant processes related to the post-Zapotecan metamorphic retrogression, and only a few whole-rock light rare element patterns display strong enrichments.

1. Introduction

The basement of eastern Mexico comprises late Mesoproterozoic-age granulite-facies metamorphic rocks (Fig. 1a), constituting the core of an inferred microcontinent named Oaxaquia (Ortega-Gutiérrez et al., 1995). The birth of proto-Oaxaquia was linked to an oceanic island arc (e.g., Weber and Schulze, 2014). Mesoproterozoic paleogeographic reconstructions for proto-Oaxaquia are related to the transition from Columbia to Rodinia supercontinents at ~1.5 Ga (e.g., Cawood and Pisarevsky, 2017; Li et al., 2008). Late Mesoproterozoic paleogeographic reconstructions locate proto-Oaxaquia interacting with the northwestern margin of the Amazonian craton in a magmatic backarc/forearc active margin (Ortega-Gutiérrez et al., 2018). This Mesoproterozoic arc-building takes place in an era of relative tectonic stability and high mantle temperatures, whereas modern arc-building systems postdate the initiation of deep subduction and mantle cooling in the later Neoproterozoic. Nevertheless, despite these differences, the arc-building mechanisms may still have been similar (e.g., Ibañez-Mejía et al., 2011).

All Mexican Grenvillian basement outcrops (Novillo Gneiss; Huiznopala Gneiss; Oaxacan Complex (OC); and Guichicovi Complex, Fig. 1b) host metamorphosed basic to intermediate mafic granulites, also called metabasites. The OC represents the largest outcrop belt (~6600 km^2) of Grenvillian-age rocks in Mexico (Fig. 1b). In the northern OC at ~1100 Ma the Olmecan event generates migmatization (Solari et al., 2003), when proto-Oaxaquia is involved in accretionary orogenesis with the NW Amazonia craton (Cawood and Pisarevsky, 2017) and at 1000–980 Ma the Zapotecan event (Solari et al., 2003) involve proto-Oaxaquia in collisional orogenesis with NW Amazonia craton (Cawood and Pisarevsky, 2017). Both Olmecan and Zapotecan events belong to the Grenvillian cycle. The Zapotecan event is

* Corresponding author at: Departament de Geologia, Universitat Autònoma de Barcelona, 08193 Cerdanyola del Vallès, Spain.
E-mail address: Laura.Culi@uab.cat (L. Culí).

https://doi.org/10.1016/j.lithos.2023.107239
Received 30 November 2022; Received in revised form 30 May 2023; Accepted 3 June 2023
Available online 8 June 2023
0024-4937/© 2023 The Authors. Published by Elsevier B.V. This is an open access article under the CC BY-NC-ND license (http://creativecommons.org/licenses/by-nc-nd/4.0/).

equivalent to the Rigolet collisional orogenesis from the E Laurentia craton (Cawood and Pisarevsky, 2017).

Proto-Oaxaquia protoliths from southern OC include volcanic arc lavas and sediments intruded by rift-related granites with U-Pb ages of 1117 ± 4 Ma (Keppie et al., 2001). In southern OC Schulze (2011) infers various magmatic arcs and two pulses of anorthosite-mangerite-charnockite-granite (AMCG) magmatism. In the Copalita arc from southern OC there are ortho-migmatites with ages between 1.4 and 1.2 Ga. In the northern OC Keppie et al. (2003a) studied two granitic-gabbroic suites intruded at ca. 1157–1130 and ~ 1012 Ma. They inferred a magmatic arc setting for the old suite and a backarc rifting above a slab window or anorogenic intercontinental rifting for the young suite. Furthermore, Keppie and Dostal (2007) studied northern OC rift-related basalts emplaced at 1.2–1.3 Ga (Fig. 2a). In northern OC there are El Catrín ortho-migmatites dated at 1106 ± 6 Ma (Solari et al., 2003).

Until recently, modeling in metabasites was limited to simple systems in subsolidus conditions, given the simplicity of solid solution models for compositionally complex minerals such as clinopyroxenes and amphiboles and the lack of an adequate solution model for melts of basic composition (Diener and Powell, 2012; Green et al., 2007). Although petrological modeling in anatectic rocks with silica-saturated compositions has been possible for >15 years due to the existence of a granitic composition melt model (White et al., 2002), only recently a set

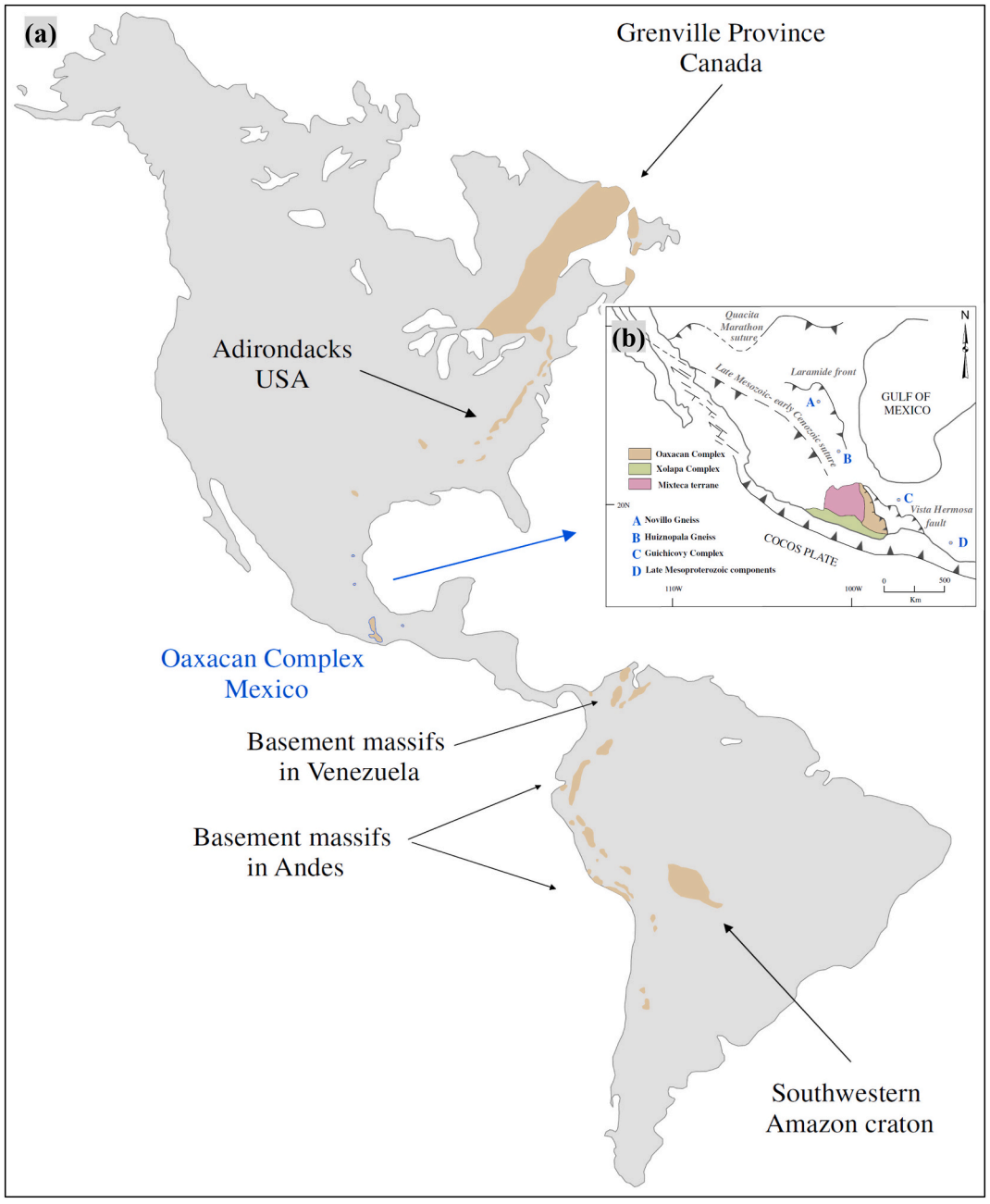

Fig. 1. a) Main Grenville-age basement rocks in North and South America, modified from Gillis et al. (2005). b) Map of Mexico showing the main geological features. The Oaxacan Complex is the largest outcrop of Grenvillian rocks in Mexico. It is in tectonic contact with the Xolapa Complex and the Mixteca Terrane. Besides the Oaxacan Complex, the four exposures of Grenvillian-age granulite-facies metamorphic rocks in eastern and southern Mexico are the Novillo Gneiss (A), Huiznopala Gneiss (B), Guichicovi Complex (C), and in the state of Chiapas, there are late Mesoproterozoic components that have been reworked by Ordovician magmatism and metamorphism (D).

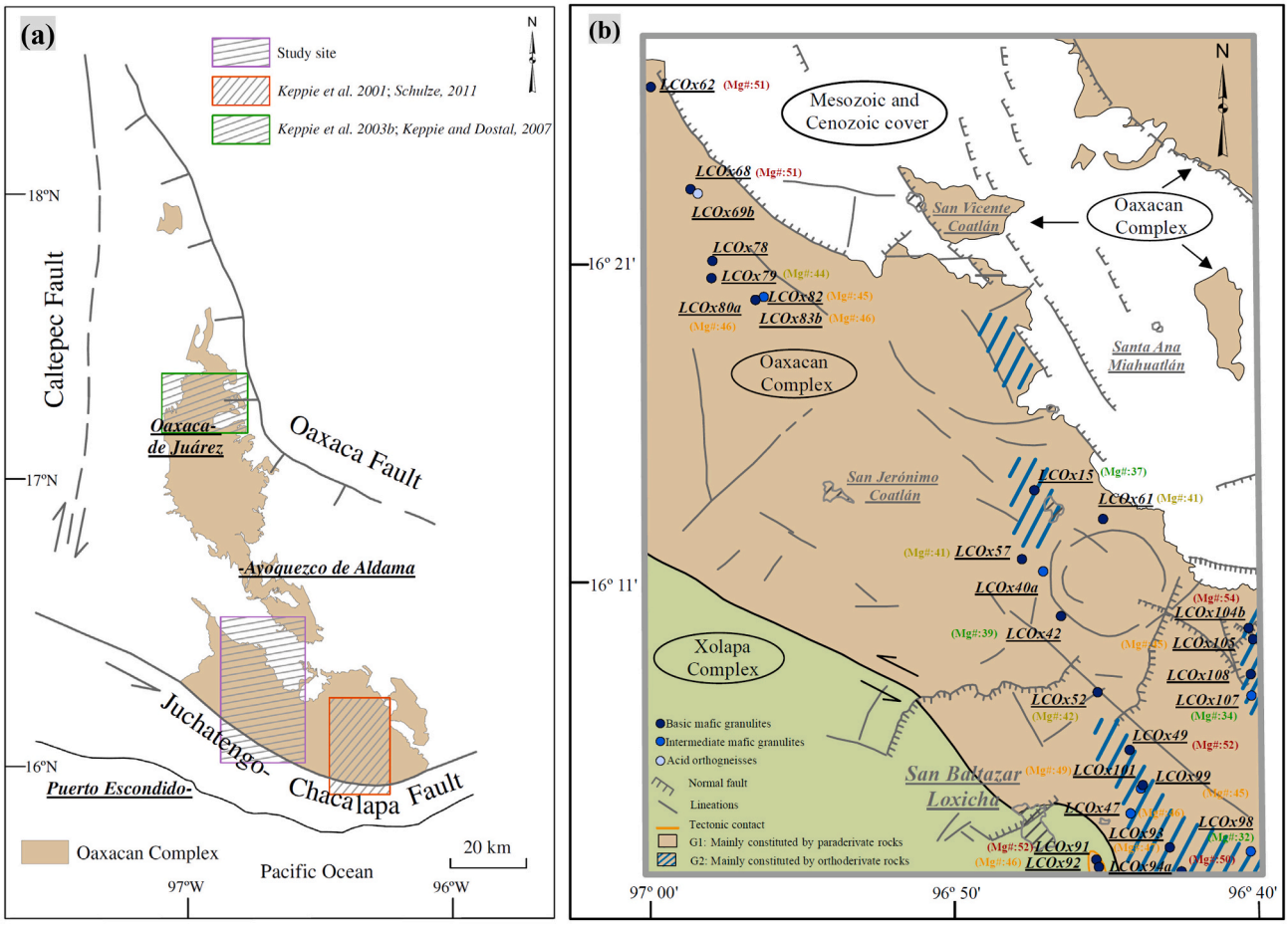

Fig. 2. a) The Oaxacan Complex (OC) of southern Mexico. The southern part of the OC studied by Keppie et al. (2001) and Schulze (2011) is marked with an orange rectangle, and the northern part of the OC studied by Keppie et al. (2003a) and Keppie and Dostal (2007) is marked with a green rectangle. The southwestern OC study site is marked with a purple rectangle. b) Simplified geological and structural map of the study area between San Vicente Coatlán and San Baltazar Loxicha with sample locations and their Mg#. Modified from 1:25000 scale geological maps of Ejutla de Crespo (Fitz-Bravo and Castillo-Reynoso, 2010) and San Baltazar Loxicha (Uribe-Luna and Pérez-Reynoso, 2012) and 1:250000 scale geological map of Zaachila (Servicio Geológico Mexicano (SGM), 2000). *Mg# = [MgO(wt%)/MgO (molec. wt)]/[Fe_2O_3t(wt%)/Fe_2O_3t(molec. wt) + MgO(wt%)/MgO (molec wt)] × 100. (For interpretation of the references to colour in this figure legend, the reader is referred to the web version of this article.)

of activity-composition (*a-x*) relations for basic melts (tonalitic-trondhjemitic) has been developed and tested with relative success in a system with sufficient complexity to approximate real behavior (e.g., Green et al., 2016; Holland et al., 2018). The models of Green et al. (2016) represent the melting of metabasite rocks, generating a melt more calcic than a typical granitic melt and pyroxene and amphibole *a-x* models have been refined and extended to the same system, making it possible to simulate the actual compositions of these minerals in granulite facies intermediate and basic rocks.

This study focuses on the basic-intermediate mafic granulites (metabasites) from southwestern OC, a sector that has never been studied in detail before and located between the previously studied northern and southern sectors. The main goals of this paper are: 1) to study for the first time the geochemistry of the southwestern OC basic and intermediate mafic granulites to infer about the protoliths' nature, the paleosetting in which they were emplaced, and the structure/geometry of the proto-Oaxaquia island/continental arc outcropping in the Zapotecan granulitic facies (last stage of Grenvillian cycle), and 2) to infer the metamorphic peak conditions of the southern OC, to decipher the existence and time of partial melting/restitic features and the post-metamorphic hydration conditions through geochemical features and phase equilibria modeling.

2. Geological setting and collected samples

The study site is in the southwestern OC between Sant Vicente Coatlán and San Baltazar Loxicha (southern Oaxaca State, México). The OC units from the study site have been divided for the first time into two main groups (G1 and G2) following a lithological criterion (Fig. 2b). The G1 group comprises mainly semipelitic granulites and quartz-feldspathic granulitic paragneisses (containing the common assemblage Fsp (perthitic) + Pl + Qz ± Opx ± Grt ± Cpx ± Sil ± Gr ± Bt and Fsp (perthitic) + Pl + Qz ± Grt ± Opx ± Sil ± Gr respectively), with some para-amphibolite and calcsilicate rocks and anatectic marbles (all abbreviations according to Whitney and Evans, 2010). G1 also contains pegmatites (Shchepetilnikova et al., 2015), basic and intermediate mafic granulites, and scarce leucosomatic and ultramafic bodies (Culí, 2020, Culí et al., 2020). Therefore, G1 is mainly constituted by paraderivate rocks. In G1, basic and intermediate mafic granulites are emplaced showing pre-metamorphic contacts (Supplementary Fig. 1a and 1 h), sometimes they occur as m-cm size intercalations (Supplementary Figs. 1b and 1c), or they are emplaced as m- to km size stocks (Supplementary Fig. 1d). The G2 is constituted by intermediate and basic mafic granulites intruded by minor pegmatites. Therefore, G2 is mainly constituted by orthoderivate rocks. In some outcrops from the southern part of the study site (G2), the mafic granulites display Grt-rich neosomes (Supplementary Fig. 1e) and m-size roof pendants of Qz-Fsp

granulitic paragneisse (Supplementary Fig. 1f).

The general foliation trend at the study site is around N 330 – N 345. The orogen has different exposed structural levels (Culí et al., 2021, 2022), and brittle deformation is represented by both normal (Supplementary Fig. 1i) and lateral faulting.

Collected samples correspond to intermediate and basic mafic granulites, containing the common assemblage Pl + Cpx ± Grt ± Amp ± Opx ± Bt ± Qz ± Fe-Ti oxides (Supplementary Table 1). Samples were collected from both G1 and G2 groups.

3. Analytical methods

Petrographic studies were carried out on thin sections using a Zeiss Axio Imager A2.m optical microscope at Laboratorio Nacional de Geoquímica y Mineralogía (LANGEM), UNAM, Mexico.

Whole-rock (WR) major element analyses were performed by conventional X-ray fluorescence (XRF) using a sequential X-ray spectrometer (Rigaku Primus II) equipped with a rhodium tube and a 30-μm beryllium window (LANGEM, UNAM). Reference material measured concentrations and detection limits are reported in Lozano and Bernal (2005) (Supplementary Table 2a).

WR trace element analysis was performed at Actlabs (Ontario, Canada). The technique used employs a lithium metaborate/tetraborate fusion. The resulting molten bead is rapidly digested in a weak nitric acid solution. Analyses were made by Inductively Coupled Plasma Mass Spectrometry (ICPMS). The samples were melted with a flow of lithium metaborate and tetraborate using an induction furnace. The glasses obtained were continuously mixed with a 5% nitric acid solution containing an internal standard until the sample was completely dissolved. Dissolved samples were analyzed with a Perkin Elmer Sciex ELAN 6000, 6100, or 9000 ICP–MS. Samples were analyzed with blank and three controls (two before the sample group and one after). The precision of trace elements analyses expressed as coefficient of variation (CV) and limit of detection (LOD) are reported in Supplementary Table 2b.

Mineral phases from modeled samples were analyzed by wavelength-dispersive electron-probe microanalysis (WDS-EPMA) at the Centre Científic i Tecnològic at the Universitat de Barcelona (CCiTUB), Spain. Analyses were performed on a JEOL JXA-8230 electron microprobe equipped with five wavelength-dispersive spectrometers (WDS) and a silicon-drift detector EDS. Spot analyses were carried out with an accelerating voltage of 15 kV, a beam current of 15 nA, and a beam spot of 5 μm. Analytical standards, crystals, and X-ray lines used were hematite (Fe, LiFH, Kα); rutile (Ti, PETJ, Kα); periclase (Mg, TAP; Kα); rhodonite (Mn, LiFH, Kα); Al_2O_3 (Al, TAP, Kα); Cr_2O_3 (Cr, PETJ, Kα); diopside (Si, TAP, Kα); wollastonite (Ca, PETL, Kα); orthoclase (K, PETL, Kα); barite (Ba, PETL, Kα) and albite (Na, TAP, Kα). Standard data on mineral analyses, including precision and accuracy, are reported in Supplementary Table 2c.

4. Results

4.1. Petrography

The intermediate/basic mafic granulites main mineral association is Pl + Cpx + Bt/Amp ± Grt ± Opx ± Fsp (perthitic) ± Qz. The basic compositions have lower contents of Fsp and Qz than intermediate compositions (Supplementary Table 1). Mafic granulites have mainly granoblastic and locally decussate textures (Fig. 3a, b, c, and d). Microperthitic Fsp indicates that it was ternary at the metamorphic peak and suggests high temperature (HT) (>700 °C) processes (Fig. 3c). There are also myrmekitic textures formed from feldspar (Fig. 3e). Most of the Pl crystals are not retrograded to sericite. Bt and Amp are highly pleochroic due to their high Ti and Fe contents. Although mainly decussate, Bt and Amp sometimes delineate a poorly defined oriented fabric (Fig. 3f and g). In some cases, skeletal Bt displays evidence of being nucleated at the expense of Cpx (Fig. 3g) in a retrograde process. In other cases, Cpx grains have formed along Amp or Amp-Pl boundaries (Fig. 3h). Therefore, the partial replacement of Amp by Cpx is a prograde process. No secondary Amp completely replacing the Cpx/Opx has been detected. Therefore, the post-magmatic/retrograde metamorphism processes are only incipient. Both Cpx and Opx are mainly allotriomorphic (Fig. 3i). Grt porphyroblasts (Fig. 3j) display subidiomorphic to allotriomorphic morphology and contain Qz, Pl, Amp, Opx, Ap, Bt, Fe-Ti oxides, or Mag inclusions (Culí et al., 2021). The accessory minerals are Zrn, Ap, and Fe-Ti oxides. Some of the studied samples belong to the charnockite series (e.g., Le Maitre, 2002) due to the amounts of Opx as one of the main mineral phases (samples in grey italics from Supplementary Table 1).

4.2. Whole-rock geochemistry

4.2.1. Major elements

Studied samples correspond to intermediate (52–65% SiO_2) and basic (45–52% SiO_2) granulites (metabasites), except for one sample (LCOx69b), which is acid (>65% SiO_2) (Supplementary Table 3a). The WR low values of LOI (Loss On Ignition) suggest no significant post-metamorphic hydration processes (e.g., Smith and Humphries, 1998).

Following, e.g., Kelemen et al. (2014), lavas, melts, and liquids with Mg# < 50 are evolved, with Mg# from 50 to 60 are high Mg#, and with Mg# > 60 are primitive (Mg# = molar (MgO/(MgO + FeO) × 100) where all iron is treated as FeO). Mg# from studied samples ranges from 34 to 53.7, belonging to the evolved and high Mg# groups (Supplementary Table 3a). LCOx69b (Mg# = 7.2), LCOx78 (Mg# = 25.5), and LCOx108 (Mg# = 65.3) samples are not considered as their values seem to correspond to outliers and are evaluated in the discussion section. The rest of the samples could be classified into four groups: 1) high Mg# group, 2) group between 45 and 49 Mg#, 3) group between 41 and 44 Mg#, and 4) group between 32 and 39 Mg# (Fig. 2b and Supplementary Table 3b).

The CIPW norm of studied samples is shown in Supplementary Table 4. The calculations were done using the spreadsheet of Naslund (2007). All samples display An, Or, Ab, Ilm, Ap, and Mag (except the LCOx108 sample) as normative minerals. Most of the samples display Hyp and those that do not display Hyp display Nph as a normative mineral (LCOx57, LCOx62, LCOx68, and LCOx92 samples). The An-Ab-Or normative diagram is shown in Supplementary Fig. 2. Almost all the samples are projected on the left-hand side of the diagram, close to the An-Ab axis.

The plutonic protoliths from the studied samples can be classified as gabbro, gabbro-diorite, monzogabbro, monzodiorites, and diorite and to samples as foid monzogabbro (TAS diagram Middlemost, 1994, Supplementary Fig. 3a), or its volcanic equivalents like basalt, basaltic andesite, andesite, trachybasalt, basaltic trachyandesite, and rhyolite and two samples as phonotefrite (TAS diagram Middlemost, 1994, Supplementary Fig. 3b).

4.2.2. Minor and trace elements

Minor and trace elements from the studied samples are shown in Supplementary Table 5a.

In Fig. 4, it can be seen how Ni and Cr values covary with decreasing Mg#. These facts suggest certain differentiation or variability from the source which generated these rocks. For example, Cortesogno et al. (2000) demonstrated that the comparison of metamorphically recrystallized gabbro under HT conditions with the literature data from non-metamorphic protoliths points to similar Mg# and modal compositions, and it suggests that the effects of element mobilization during ductile events are moderate on the WRs. Furthermore, Andersson et al. (2006) demonstrated that decreasing Ni and Cr values covary with decreasing Mg# for their studied metabasite rocks, so these elements cannot distinguish between high-grade and low-grade metamorphic rocks. Finally, Treloar (1987) demonstrates that while Cr may be mobile in hydrothermal systems, it is immobile under metamorphic conditions.

Zr/Nb, Th/Nb, and Th/La ratios from the studied samples point to

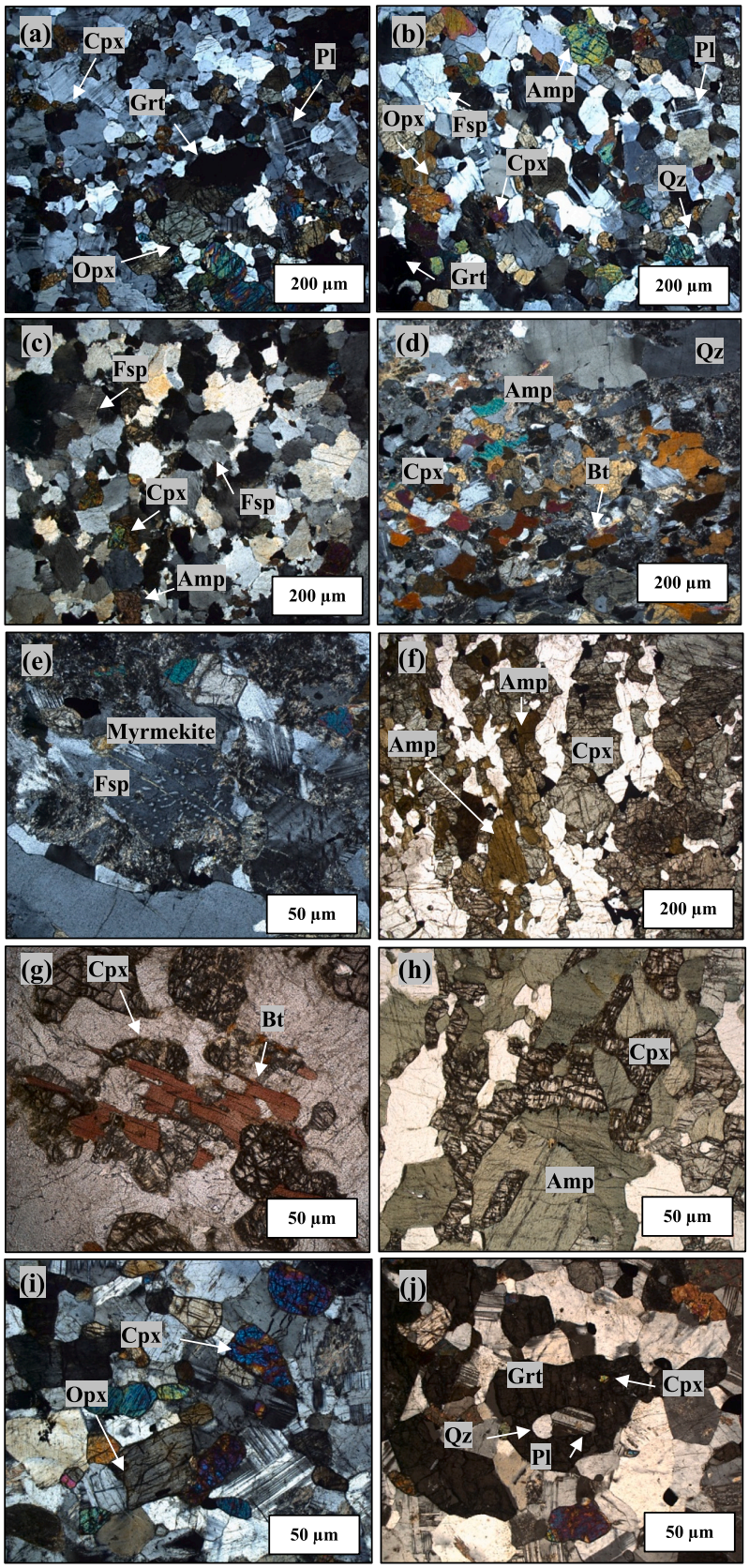

Fig. 3. Optical microscope images of southwestern Oaxacan Complex mafic granulites: a) General view of granoblastic texture in crossed nicols from intermediate mafic granulite (LCOx78). b) General view of granoblastic texture in crossed nicols from basic mafic granulite (LCOx101). c) General view of granoblastic texture with perthitic feldspar in crossed nicols from intermediate mafic granulite (LCOx47). d) General view of granoblastic texture in crossed nicols from basic mafic granulite (LCOx68). e) Myrmekitic textures formed from feldspar in crossed nicols from basic mafic granulite (LCOx15). f) Pleochroic Amp defining the rock lineation in plane-polarized light from basic mafic granulite (LCOx79). g) Skeletal Bt in crossed nicols from mafic granulite (LCOx49). h) Cpx formed along Amp or Amp-Pl boundaries in plane-polarized light from intermediate mafic granulite (LCOx54). i) Subidiomorphic Opx and Cpx in crossed nicols from intermediate mafic granulite (LCOx99). j) Grt blastopoikilitic of Pl, Cpx, and Qz in crossed nicols from basic mafic granulite (LCOx94b).

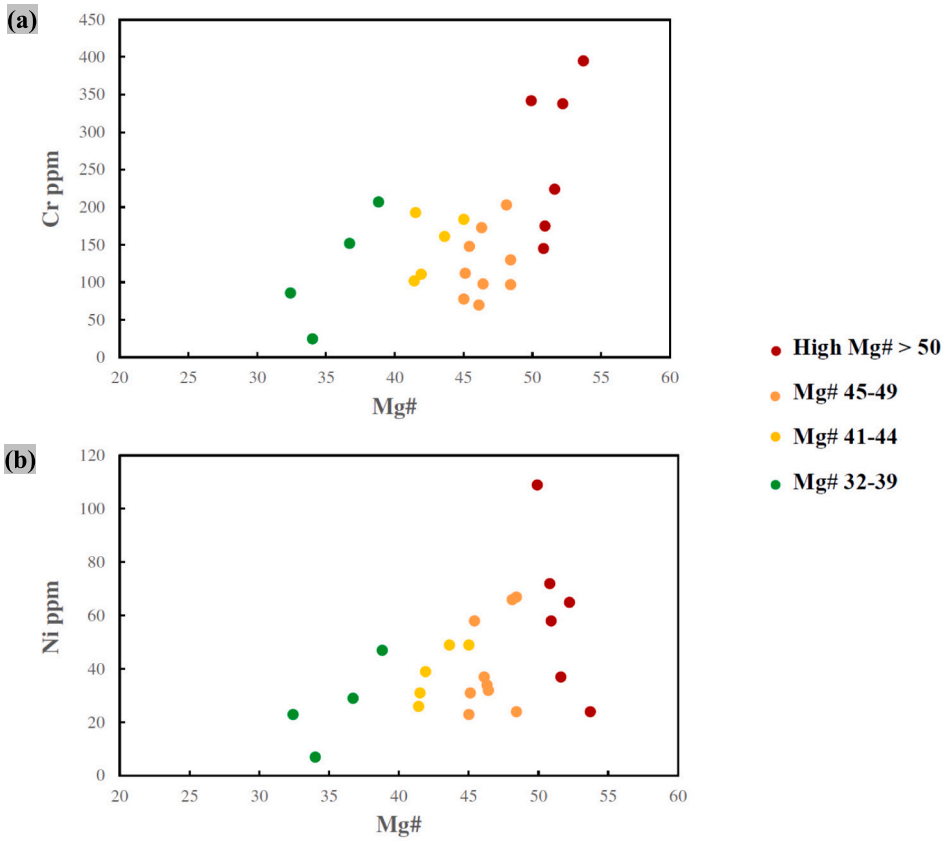

Fig. 4. Ni and Cr (ppm) against Mg# (mol %) as an evolution index in southwestern OC samples. *Mg# = [MgO(wt%)/MgO (molec. wt)]/[Fe_2O_3t(wt%)/ Fe_2O_3t (molec. wt) + MgO(wt%)/MgO (molec wt)] x 100.

depleted mantel (DM) sources (Salters and Stracke, 2004), and La/Nb, Ba/Nb, Rb/Nb, and Ba/La ratios mainly to middle continental crust sources (Rudnick and Gao, 2014) (Supplementary Table 5b). Therefore, the studied mafic granulites reflect both mantle and crustal sources.

Fig. 5a displays the minor and trace element patterns of the studied samples normalized to the chondritic uniform reservoir (CHUR, Sun and McDonough, 1989). This figure shows the normal (N)-MORB, enriched (*E*)-MORB, and oceanic island basalts (OIB) from Sun and McDonough (1989) and the lower and middle continental crust from Rudnick and Gao (2003). In this figure, most samples display trace element concentrations like those of OIB and the middle continental crust. However, three samples (LCOx15, LCOx49, and LCOx47) have higher rare-earth element (REE) concentrations than those from OIB. On the other hand, one sample displays lower REE concentrations than those of N-and *E*-MORB and lower continental crust (LCOx80a), and two samples display similar REE concentrations to N and *E*-MORB (LCOx104b and LCOx108). Apart from that, some WR samples (LCOx15, LCOx47, LCOx49, and LCOx61, Fig. 5a) display much higher concentrations of light (LREE) than heavy REE (HREE). These facts are assessed in the discussion section.

Fig. 5b displays the minor and trace patterns normalized to the primitive mantle (PM, Sun and McDonough, 1989). This figure shows the N-MORB, *E*-MORB, and OIB from Sun and McDonough (1989) and the lower and middle continental crust from Rudnick and Gao (2003). In this figure, like Fig. 5a, most samples display trace element concentrations relatively similar to those of OIB and the middle continental crust. However, three samples (LCOx15, LCOx49, and LCOx47) have higher trace element concentrations than those from OIB. On the other hand, some samples display trace element concentrations like N-MORB and E-MORB (LCOx78, LCOx80a, LCOx83b, LCOx99, and LCOx108), especially between the elements Rb and Sr (middle of the left part of Fig. 5b). Besides, all studied mafic granulites/metabasites display negative Th, Nb, and positive Ti anomalies (only the LCOx49 sample has no Ti anomaly). Finally, as a generalization, incompatible elements which belong to the low field strength LILE group (Cs, Rb, K, Ba, Sr, Eu, and Pb) are fluid mobile (e.g., Rollinson and Pease, 2021). All studied samples display positive Ba anomalies. This fact is assessed in the discussion section.

In this study, we use geotectonic diagrams consistent with the nature of the protoliths and involving low mobility elements because our samples were subjected to high metamorphic conditions. Depending on the tectonic diagram used, studied samples are plotted in different fields: 1) IAB, MORB, and within-plate basalts (WPB) (Pearce and Norry, 1979, Fig. 6a). 2) Plume-influenced MORB field (P-MORB). This type is equivalent to the E-MORB (Meschede, 1986, Fig. 6b). However, some samples fall in the within-plate tholeiites (WPT) and within-plate alkali basalts (WPA) field, and one sample (LCOx83b) is in the volcanic arc basalt (VAB) field. 3) E-MORB, N-MORB, P-MORB, and alkaline basalts (AB) related to the MORB-OIB array (divergent margins), and calc-alkaline basalts (CAB), backarc basin basalts (BABB), and island arc tholeiitic (IAT)-Boninite field, related to the volcanic arc array (convergent margins) (Saccani, 2015, Fig. 6c).

4.3. Phase equilibria modeling

A remarkable prediction of pseudosection modeling using the new *a-x* relations, as stated by Green et al. (2016) and Palin et al. (2016b), is that in basic and intermediate rocks of varied composition (OIB and MORB basalts, diorites), with enough hydration the solidus should occur under amphibolite facies conditions in a very limited range of T: 690–695 °C at 0.5 GPa. The first appearance of Opx (and therefore the transition to granulite facies) would also occur in a limited range:

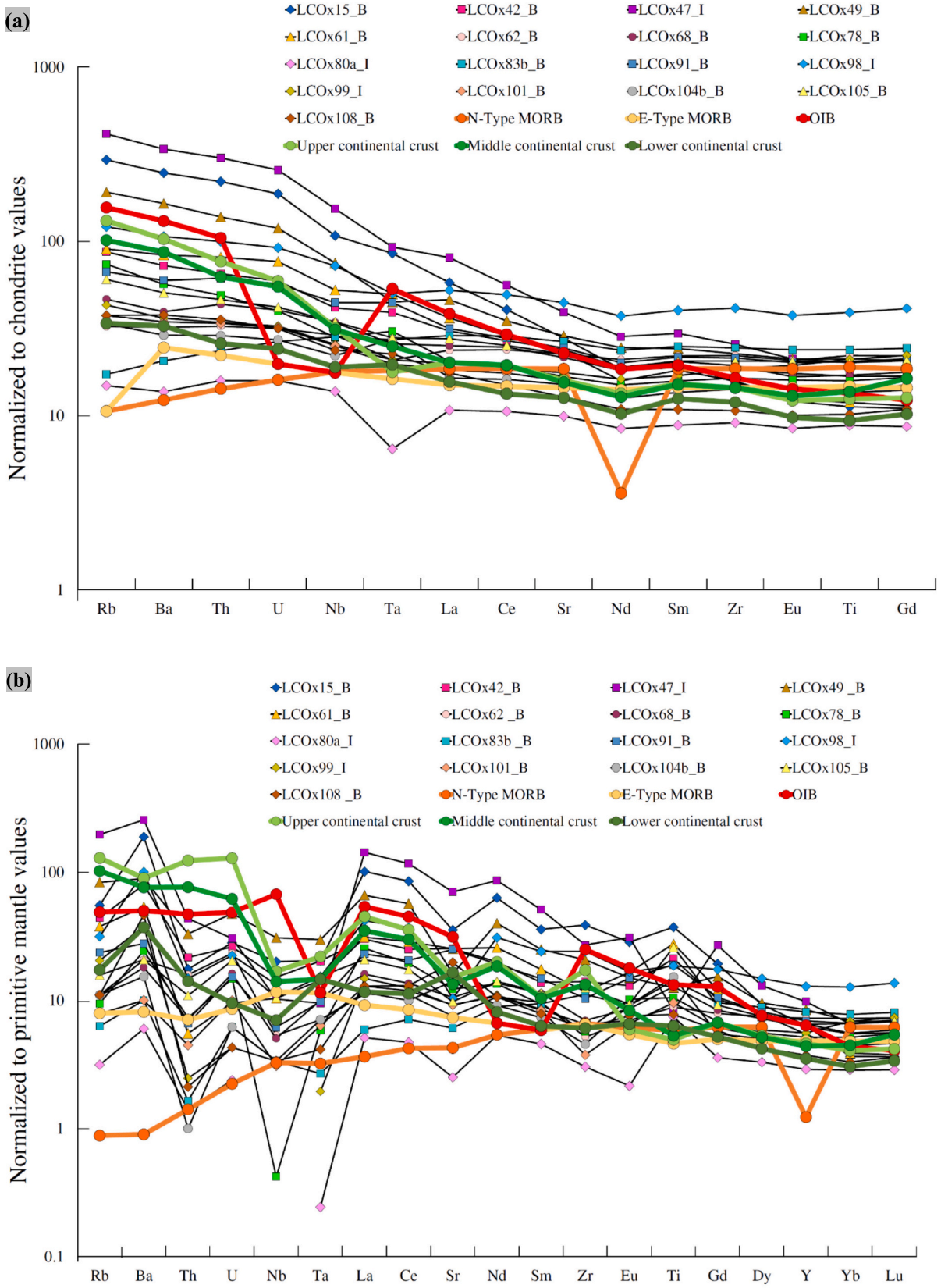

Fig. 5. a) The minor and trace element patterns of the studied samples normalized to the chondritic uniform reservoir (CHUR, Sun and McDonough, 1989). This figure shows the N-MORB, E-MORB, and OIB from Sun and McDonough (1989) and the lower and middle continental crust from Rudnick and Gao (2003). b) The minor and trace element patterns normalized to the primitive mantle (PM, Sun and McDonough, 1989). This figure shows the N-MORB, E-MORB, and OIB values from Sun and McDonough (1989) and the lower and middle continental crust from Rudnick and Gao (2003). *B=Basic and I=Intermediate.

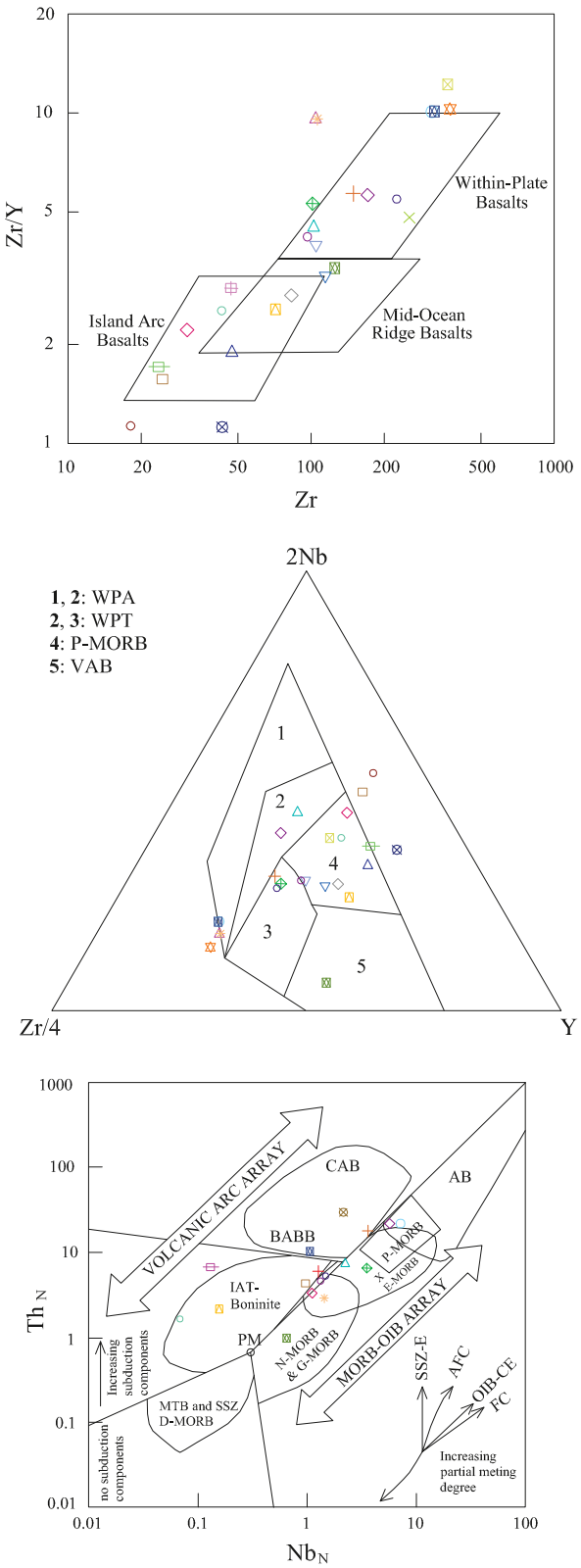

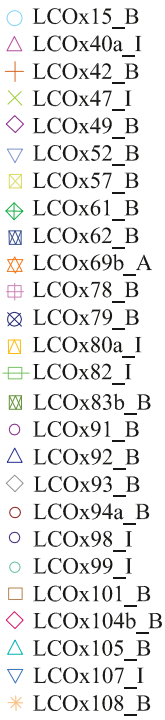

Fig. 6. Geotectonic diagrams. a) Bivariate diagram of Zr vs. Zr/Y of Pearce and Norry (1979). b) Trivariate diagram of Zr/4 – 2Nb – Y of Meschede (1986). c) Bivariate diagram of Nb normalized vs. Th normalized of Saccani (2015). *WPB: within-plate basalts; WPA: within-plate alkali basalts; WPT: within-plate tholeiites; MORB: Mid- Ocean ridge basalts; E-MORB: enriched MORB; P-MORB: Plume-influenced MORB; IAB: island arc basalts; VAB: volcanic arc basalts; AB: alkaline basalts; CAB: calc-alkaline basalts; BABB: back-arc basin basalts and IAT: island arc tholeiites. B=Basic; I=Intermediate and A = Acid.

800–825 °C. The high-T limit for the amphibole stability field is highly dependent on composition and occurs between 1025 and 1040 °C for metabasalts but at 805–825 °C for metadiorites. The composition of the generated melt evolves from a first, scarce melt of granitic composition at near solidus T to melts of either trondhjemitic-tonalitic or granodioritic composition in metabasalts and metadiorites, respectively (Palin et al., 2016). In a closed system, where the melt could not migrate outward and remain in situ, granulite associations should destabilize to subsolidus associations containing Hb + Pl ± Bt ± Qz ± H_2O during retrogression. The high prevalence of granulite mineralogical preservation (with Opx) suggests that in nature, migration and loss of melts (and so of water) out of the system prevent the destabilization of

granulite-facies assemblages (Powell and Downes, 1990). Apart from that, the high proportion of melts generated in the closed hydrated system will result in mechanical instability, making the situation rheologically unfeasible (e.g., Renner et al., 2000), so their retention would be physically impossible, and massive melt migration will be the most probable scenario. Melting under highly hydrated conditions would, in principle, be unlikely in mid-lower crustal conditions at high P and with low intergranular porosity, although exceptionally, they could occur during localized infiltration of H_2O-rich fluids. Palin et al. (2016b) also show how the stabilization of granulite facies assemblages (with Opx) in metabasalts is theoretically possible also in subsolidus conditions even if the proportion of aqueous fluid is low (ca. <4.5% molar H_2O) or the H_2O is diluted in a multicomponent fluid, generating a low f(H_2O) condition.

4.3.1. Mineral phase association, whole-rock composition, and modal analysis from modeled samples

The modeled samples belong to G1 and correspond to one Grt-Amp-bearing basic mafic granulite (LCOx61 sample) and one Amp-bearing basic mafic granulite (LCOx62 sample) (Supplementary Fig. 1 and samples in black italics, Supplementary Table 1).

4.3.1.1. Grt-Amp bearing basic mafic granulite (LCOx61 sample). The mineral association of this sample is Pl ($An_{50–70}$) + Cpx (Aug) + Amp (Prg) + Grt ($Alm_{54-56}Py_{22–24}Grs_{18-19}Sps_{2.3–2.6}$) + Opx (En) ± Qz ± Ilm ± Zrn ± Ap. The texture of this rock is granoblastic (Fig. 7a). The boundaries between mineral phases are straight. They do not display deformational features and almost no reactional textures related to metamorphic retrogression (Fig. 7b). Grt with Cpx and Amp inclusions display resorbed borders (Fig. 7c). Mineral analysis from the LCOx61 sample includes rim-core-rim profiles and is shown in Supplementary Table 6a.

4.3.1.2. Amp-bearing basic mafic granulite (LCOx62 sample). The mineral association of this sample corresponds to Amp (Prg) + Pl (Ab) + Cpx ± Opx ± Bt ± Qz ± Ilm ± Mag ± SFe (Py). Its texture is granonematoblastic, and Amp defines the foliated fabric (Fig. 7d). Fig. 7e shows Cpx and Mag, and Fig. 7f shows a relict Opx. Mineral analyses from the LCOx62 sample include rim-core-rim profiles and is shown in

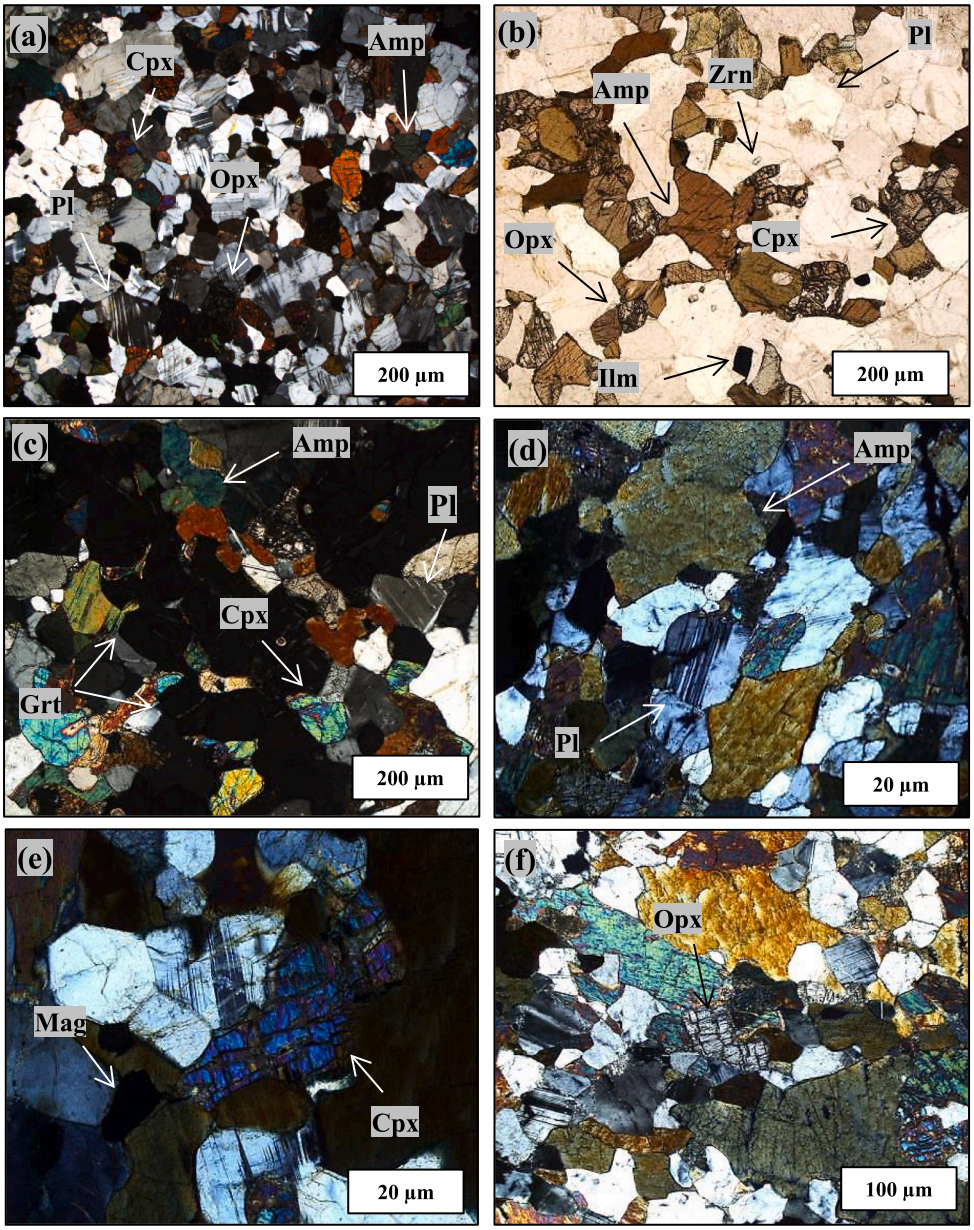

Fig. 7. a) Granoblastic texture from the LCOx61 sample. b) The boundaries between mineral phases from the LCOx61 sample are straight and do not display deformational features and almost no reactional textures related to metamorphic retrogression. c) Grt with Cpx and Amp inclusions and resorbed borders from the LCOx61 sample. d) Granonematoblastic texture and Amp defining the foliated fabric from the LCOx62 sample. e) Cpx and Mag from the LCOx62 sample. f) A relict Opx from the LCOx62 sample.

Supplementary Table 6b. This sample can be classified as an Amp-bearing (retrograde) basic granulite. The Ni (110 ppm) and Cr (260 ppm) from this sample (Supplementary Table 5a) point to an ortho-derivate origin following Leake (1964).

Good knowledge of the equilibrium WR composition of the domain to be considered (effective bulk composition, Stüwe, 1997) and the equilibrium modal proportions of mineral phases (volume %) is essential. The WR and modal analysis of the modeled samples are shown in Supplementary Tables 3a and 7, respectively.

4.3.2. *P-T pseudosection modeling*

The thermodynamic phase equilibrium models consist of T-*x* and P-T pseudosections for the modeled sample compositions in the NCKFMASHTO system. The Theriak-Domino software (De Capitani and Petrakakis, 2010), the thermodynamic database ds6.2 of Holland and Powell (2011), and the *a-x* metabasite set of models from Green et al. (2016) were used. The thermodynamic database ds6 and the *a-x* relations were adapted to the Theriak-Domino software by D.K. Tinkham and are used as in Jorgensen et al. (2019). In the Green et al. (2016) metabasite set, minerals treated as pure phases are Qz, Ttn, Rt, and Lws. The a-*x* models used for solid solution phases correspond to clinoamphibole, clinopyroxene and melt (Green et al., 2016), orthopyroxene (White et al., 2014a, 2014b), garnet (White et al., 2014b), feldspar (Holland and Powell, 2003), biotite, muscovite and chlorite (White et al., 2014a), epidote (Holland and Powell, 2011), spinel (White et al., 2002) and ilmenite (White et al., 2000).

Based on the absence of significant amount of leucosomes, we should assume that no significant melting and only recrystallization of former mafic protoliths at granulitic conditions has taken place. Also, the fact that no significant retrograde features are observed precludes significant hydration in sub-solidus retrograde conditions. To obtain the P-T conditions for this recrystallization event in P-T space using an NCKFMASHTO model, we should first estimate the amount of H_2O and Fe^{3+} present in the bulk rock. Culí et al. (2021) had previously applied the Grt - Opx - Pl - Qz (LCOx61) and Culí (2020) Pl – Amp (LCOx62) geobarometers and concluded that P should be around 1GPa for LCOx61 sample and around 0.8 GPa for LCOx62 sample. Then the first modeling step consisted of carrying out T-$x(H_2O)$ and T- $x(Fe^{3+})$ pseudosections for the appropriate P conditions in both samples so we can estimate the range of H_2O and Fe^{3+} bulk contents that are coherent with the observed assemblages having stabilized near the solidus. The derived H_2O values were around 0.5% H_2O (Supplementary Fig. 4a) and 12% Fe^{3+} for the LCOx61 sample. In LCOx62 sample, we deduced a higher degree of hydration around 4% H_2O (Supplementary Fig. 4b) (coherent with a greater modal amount of Amp Supplementary Table 7). For LCOx62 sample, the amount of Fe^{3+} could not be constrained so accurately given that a range of Fe^{3+} values between 10 and 20% of Fe^{3+} are equally consistent with the observed assemblage having stabilized near the solidus. Values of molar H_2O (deduced in this way) are similar to LOI values, (Supplementary Table 3a). Given that Amp is the main hydrated phase (there are only negligible amounts of Bt), the water content for both samples were independently estimated via Amp composition (analyses of F, Cl) and mass-balance considerations using phase compositions and modes through tcsetup spreadsheet (Waters, Oxford University, personal communication). The bulk hydration values obtained from these calculations were not significantly different from those obtained from T-$x(H_2O)$ diagram considerations. We also performed P-T pseudosection diagrams assuming water-saturated solidus conditions. Those are sometimes assumed during prograde metamorphism without specific knowledge of the actual degree of hydration. According to T-$x(H_2O)$ pseudosections (Supplementary Fig. 4a and 4b) the H_2O-saturated solidus is produced at ca. 12H = 6% H_2O for LCOx61 at 1.0 GPa and 10H (5% H_2O) for LCOx62 at 0.8 GPa. In such a scenario, the observed assemblages would not have stabilized until conditions well above the solidus, as shown in P-T pseudosections using those high-water contents (Supplementary Figs. 4c and 4d). In the case of no melt mobilization (which would have been impossible given the high proportions of melt predicted in such conditions), the solid phases should have reacted with this melt allowing retrograde processes to occur without preserving of the observed assemblages (Powell and Downes, 1990). Mobilization and melt loss (which would have been probable in this case) would have probably produced some or many leucosomes that are not observed in the field.

P-T pseudosection coherent with preservation of observed assemblages near the solidus in both samples is obtained using the deduced (see above) less-hydrated conditions (Figs. 8 and 9). As for Fe^{3+} contents we finally used 12% Fe^{3+} in both samples. This value is also coherent with preservation near the solidus in both samples. Higher degrees of oxidation (until 20%) Fe^{3+} are equally coherent in the case of sample LCOx62, but we found no reliable criterium to decide any particular value on the range 12–20% Fe^{3+}, in the absence of wet analyses or Mössbauer determinations. The arrow in Fig. 8 signals the very narrow stability field for the observed assemblage in LCOx61. The measured modes and mineral compositions for LCOx61 have been compared with those predicted by the model in the narrow field and display good agreement.

The close to the solidus (thus prone to preservation) stabilization of the observed assemblage (without Opx) in the LCOx62 sample (Fig. 9) can only be achieved in the pseudosection models using higher degrees of hydration (around 4% H_2O). The P-T pseudosection performed for the overall composition of the LCOx62 sample with 4% H_2O and 12% $Fe^{3+}$is shown in Fig. 9, where, the model assemblage that best resembles the observed assemblage in this sample lacks Opx and has Bt. Anhedral Opx is present in minor amounts (1.4%) in LCOx62, and Bt is completely absent. As seen in the model, Opx appears around 620–650 °C, <0.7 GPa, suggesting that this phase can be a retrograde product, but no retrograde textures implying production of this mineral are observed. The amounts of Bt predicted by the model are much larger than the observed ones. These discrepancies can probably be assigned to over and underestimation of element contents by the solution models used and should be produced during retrogradation, which is not observed in the LCOx62 sample. For example, for the Amp rich LCOx62 sample, overestimation of Al and underestimation of Si in Amp can lead to anomalies in modal amounts: underestimation of Hb and overestimation of Cpx (Forshaw et al., 2019). Also, F and Cl are not modeled. Those elements are known to increase the stability field of Amp and its modal amounts. K in Amp is underestimated by the solution model of this mineral, and more K in Amp would imply less Bt in the model (so adjusting better to what is observed).

4.3.3. *Model testing. Comparison of the measured vs. calculated modal percentages*

For the LCOx61 sample, the measured vs. calculated modal proportions (in vol%) of Grt, Opx, Cpx, and Amp have been compared (Fig. 10a). Similarly, for the LCOx62 sample, the measured vs. calculated modal proportions (in vol%) of Cpx, Pl, Amp, and Bt were compared (Fig. 10b). A reasonable agreement arises in the comparisons between model and reality in both samples so we can consider the models and the conditions (hydration and oxidation levels) assumed previously to modeling to be realistic. Nevertheless, note that for the LCOx62 sample (Fig. 10b), the most plausible model assemblage lacks Opx, whereas the Opx is observed (although in minor amounts of around 1% vol. percent, see Supplementary Table 7) in microscope slides (Fig. 7f). Opx model stability is sensitive to H_2O content. This fact can be seen in the T-$x(H_2O)$ diagram of Supplementary Fig. 4b that we use to choose the amount of H_2O for constructing the P-T pseudosection for this sample (Fig. 9). We choose values of $x(H_2O)$ around 3% (H6) instead of 4% (H8) we would have stabilized Opx in the model in a very small stability field at around 900 °C. So probably, the real assemblage is slightly less hydrated than we assumed using the T-$x(H_2O)$ at 0.8 GPa method. Therefore, it is possible that the hydration episode of this sample was already prior to the solidus, i.e., before melting the sample

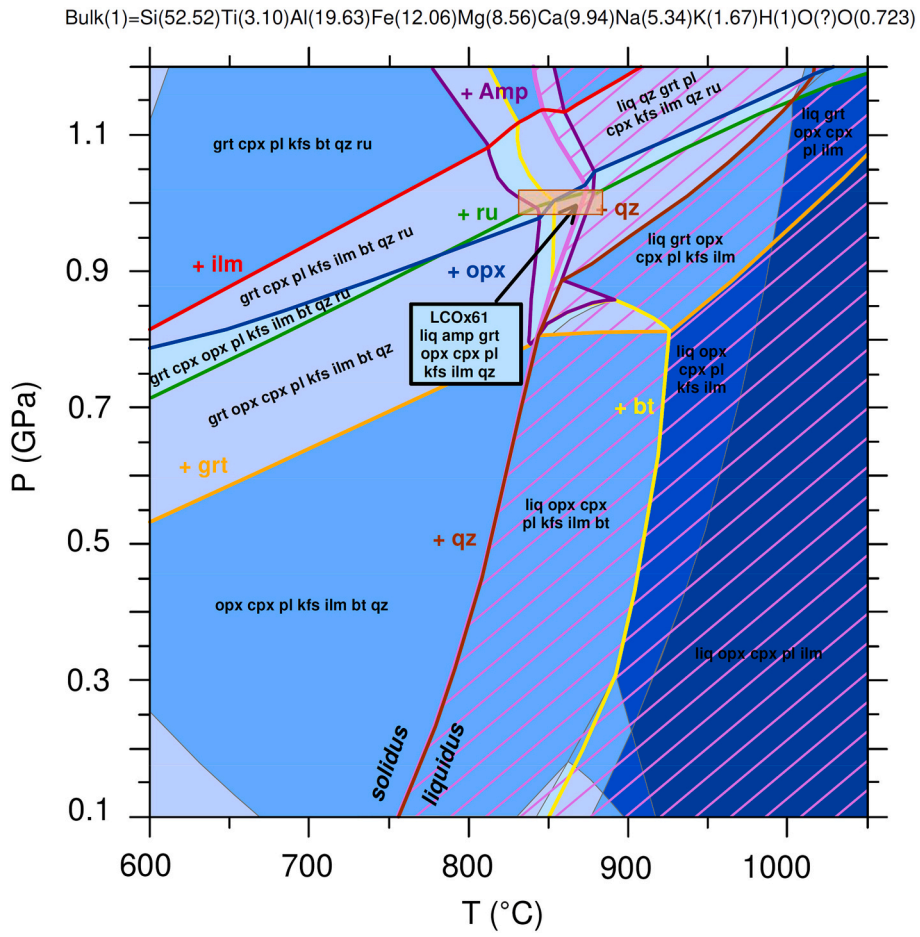

Fig. 8. P-T pseudosection calculated for Grt-Amp bearing basic mafic granulite (LCOx61). The star indicates the reference P-T conditions based on the observed mineral assemblage, and the square indicates a range of 1.0 ± 0.15 GPa and 850 ± 25 °C around this point.

could have contained Opx, then could have followed a destabilization during hydrous melting. On the other hand, Bt model amounts from the peak model assemblage in the LCOx62 sample (Fig. 10b, about 5.2%) are higher than observed.

4.3.4. Model testing. Comparison of measured and calculated mineral compositions

By constructing mineral composition isopleth diagrams, a comparison of the real mineral compositions obtained by EPMA-WDS with those predicted by the model can be made. For the LCOx61 sample, the mineral composition isopleths of Mg# = (Mg/Mg + Fe) in Grt, Cpx, Amp, and Pl (Fig. 11a) were compared. On the other hand, the model predicts the mineral typology (Grt-Alm: almandine, Cpx-Di: diopside, Amp-Prg pargasitic, and Pl-Ab: high T albitic), and this matches the classification of the real mineral phases (Supplementary Table 6a). For the LCOx62 sample, the mineral composition isopleths of Mg# = (Mg/Mg + Fe) in Amp and Pl (Fig. 11b) were compared, resulting in good agreement. The predicted mineral typologies are also concordant with the real ones. Comparison of the values obtained in the model (arrow in Fig. 8 and star in Fig. 9) with the real measured values results in a high degree of similarity. This fact suggests that the assumed hypotheses in the construction of the models (mineral associations in equilibrium, the overall compositions of the samples, and in particular, their molar ratios of H_2O, Fe^{3+}) are close to adequate, and the associations would correspond to stabilization under granulitic facies P-T conditions of two domains having undergone different proportions of melt loss.

5. Discussion

5.1. Petrography and geochemistry of the southwestern Oaxacan complex basic and intermediate mafic granulites

Petrographic textures from studied samples do not reveal remarkable post-magmatic/metasomatic processes due to the absence of Pl crystals retrograded to sericite and secondary Amp replacing the Cpx/Opx.

All studied samples display much higher amounts of normative An and Ab than Or (except LCOx47 and LCOx57 samples) in the An-Ab-Or diagram (Supplementary Fig. 2). Their plutonic protoliths are mainly gabbro and gabbro-diorite, and volcanic protoliths mainly correspond to basalt and basaltic andesite (Supplementary Figs. 3a and 3b). The high normative An and Ab can be because the studied metabasites —linked to the island arc or continental magmatic arc of proto-Oaxaquia— crop out much more in the southwestern than other parts of the OC (assuming that it is all part of the same tectonic system), or may be due to its semi-restitic character (K is one of the most mobile elements when partial melting occurs, e.g., Rudnick, 1992; Palin et al., 2016). On the other hand, samples with Or > An and Ab correspond to intermediate (LCOx47) and basic (LCOx57) orthogneisses. Their plutonic protoliths are monzodiorite-monzonite (LCOx47) and foid monzo gabbro (LCOx57), and their volcanic protoliths are trachyandesite (LCOx47) and phonotephrite (LCOx57). These samples are only found in G1 (Fig. 2b) via intercalations with paraderivate rocks. They probably belong to the shoshonitic series (e.g., Le Maitre, 2002) linked to the post-spreading stage to the backarc basins (e.g., Yang et al., 2020) related to proto-Oaxaquia. It should be emphasized that although these rocks are

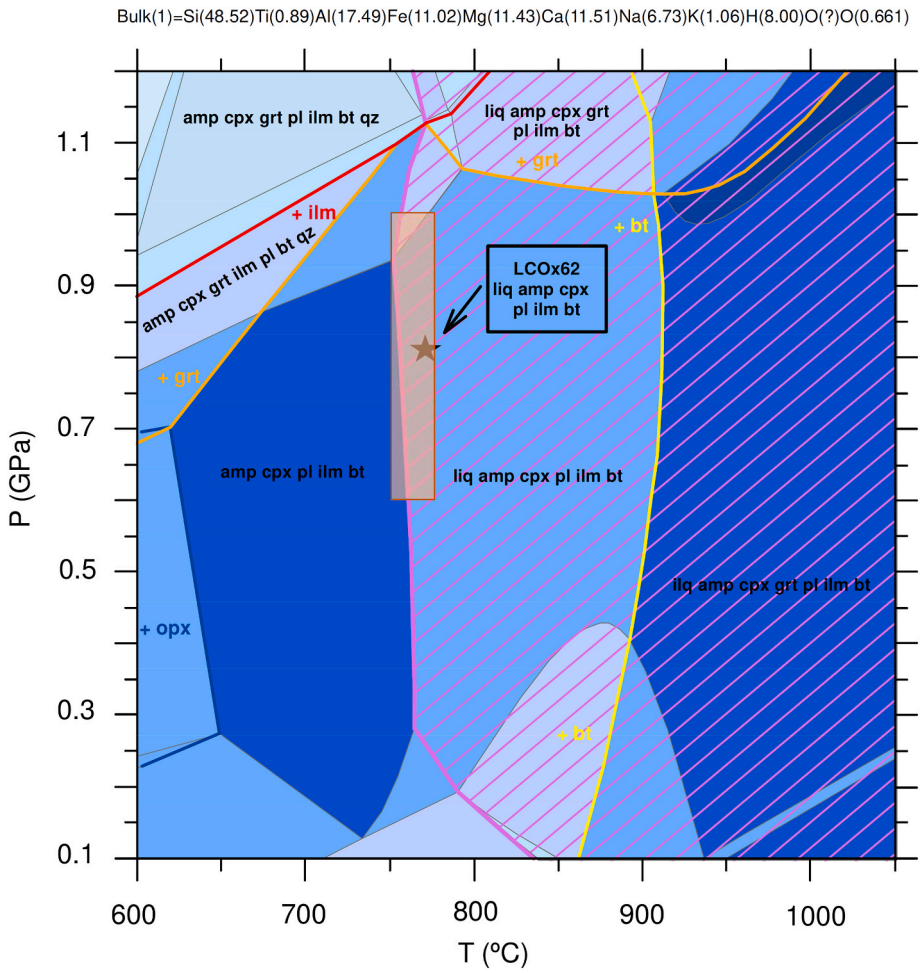

Fig. 9. P-T pseudosection calculated for Amp-bearing basic mafic granulite (LCOx62). The star indicates the reference P-T conditions based on the observed mineral assemblage, and the square indicates a range of 0.8 ± 0.2 GPa and 760 ± 10 °C around this point.

scattered in the study site, they are elsewhere in the OC.

Besides, a consistent evolutionary trend for our population of metabasites (mainly gabbro/basalt, Supplementary Figs. 3a and 3b) results in the correlation of Ni and Cr with Mg# (Fig. 4). The partly evolved Mg# (<50) and the concomitant decrease in Cr and Ni suggest that these metamorphic rocks have experienced a marked pre-emplacement fractionation of olivine and pyroxene (e.g., Andersson et al., 2006). In contrast, only rocks with relatively evolved compositions have intruded proto-Oaxaquia arc/backarc. Cr and Ni neither increase nor decrease with respect to Ti (one of the most mobile elements in the lower crust, e.g., Rollinson and Pease, 2021), informing about the nature of the protoliths.

Another interesting fact is that if the southwestern OC metabasites are plotted together with the samples from the OC southern and northern sectors studied by different authors (Keppie et al., 2001; Keppie et al., 2003; Keppie and Dostal, 2007; Schulze, 2011) in the Zr/TiO_2 vs. SiO_2 (wt%) diagram (Winchester and Floyd, 1977), southwestern OC rocks are mainly plotted in the subalkaline basalt field and few samples in an andesite field. Some of the studied samples display an affinity with Pluma de Hidalgo samples studied by Schulze (2011) from southern OC (lilac circles in Fig. 12). One sample from the southwestern OC display an affinity with two samples belonging to the upper thrust from the northern OC (Keppie et al., 2003, yellow circles in Fig. 12). Two samples from the southwestern OC display an affinity with two samples from southern OC (Keppie et al., 2001). However, only the southwestern OC studied samples, ca. half, have the lowest Zr/TiO_2 and SiO_2 contents and are projected into the subalkaline basalt field in the lower left part of the diagram. This fact shows strong evidence that the southwestern metabasites from OC constitute an assemblage apart from the rest of the OC metabasites due to their chemistry. The SiO_2 depletion of its metabasites reports restitic features for some of its samples, corroborated by their low LOI contents from WRs.

DM and middle continental crust sources are reflected via Zr/Nb, Th/Nb, Th/La and La/Nb, Ba/Nb, and Rb/Nb ratios (Supplementary Table 5b). These results are consistent with the fact that the mantle is the source of magmas related to the proto-Oaxaquia oceanic island arc and with cortical processes associated with the Grenvillian orogeny.

Referring to the highest Ba/Th ratios (Supplementary Table 5b), partial melting of the lower continental crust produces depletion of both (e.g., Rollinson and Pease, 2021). However, being depleted in Ba corresponds to ca. < 300 ppm and in Th ca. < 2 ppm (e.g., Rudnick, 1992). If Supplementary Table 5a is examined, Th values from studied samples are in the range, but the Ba values are very high.

Therefore, it is also important to look at the Ba and Th values separately for an in-depth study. For example, in the LCOx61 modeled sample, Ba values are very high, and the Th values are relatively normal. For the LCOx62 modeled sample, both Ba and Th values are in the normal range for these lithologies (Supplementary Table 5a). In other words, when viewed separately, the LCOx62 sample is depleted in these elements, and LCOx61 is slightly above the normal depletion values for these elements. This situation occurs in half of the studied samples. The other samples (LCOx15, LCOx47, LCOx49, and LOCx98, Supplementary Table 5a) display very high Ba values, so their composition indicates that they have partial melt geochemistry. This fact corroborates that the

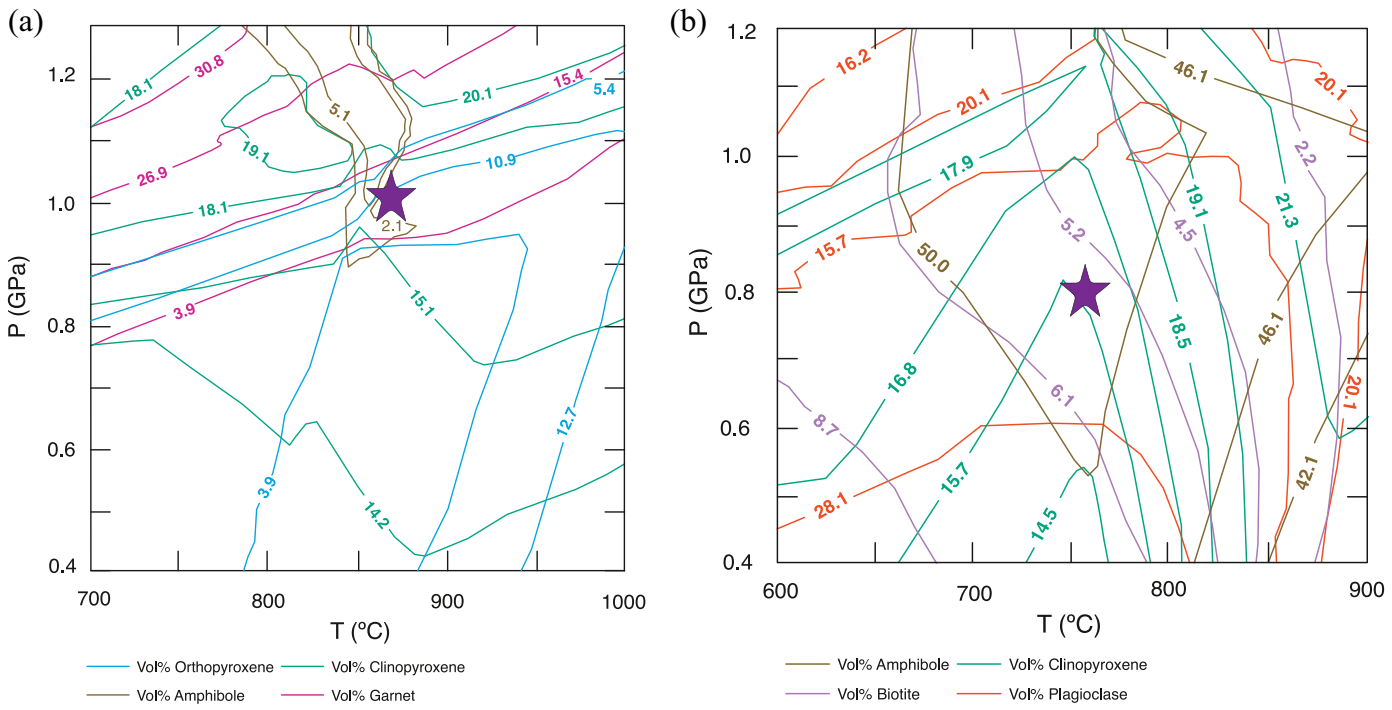

Fig. 10. a) Simplified pseudosection with molar proportions of Amp, Opx, Grt, and Cpx (in vol%) for the LCOx61 sample. b) Simplified pseudosection with molar proportions of Bt, Amp, Pl, and Cpx (in vol%) for the LCOx62 sample.

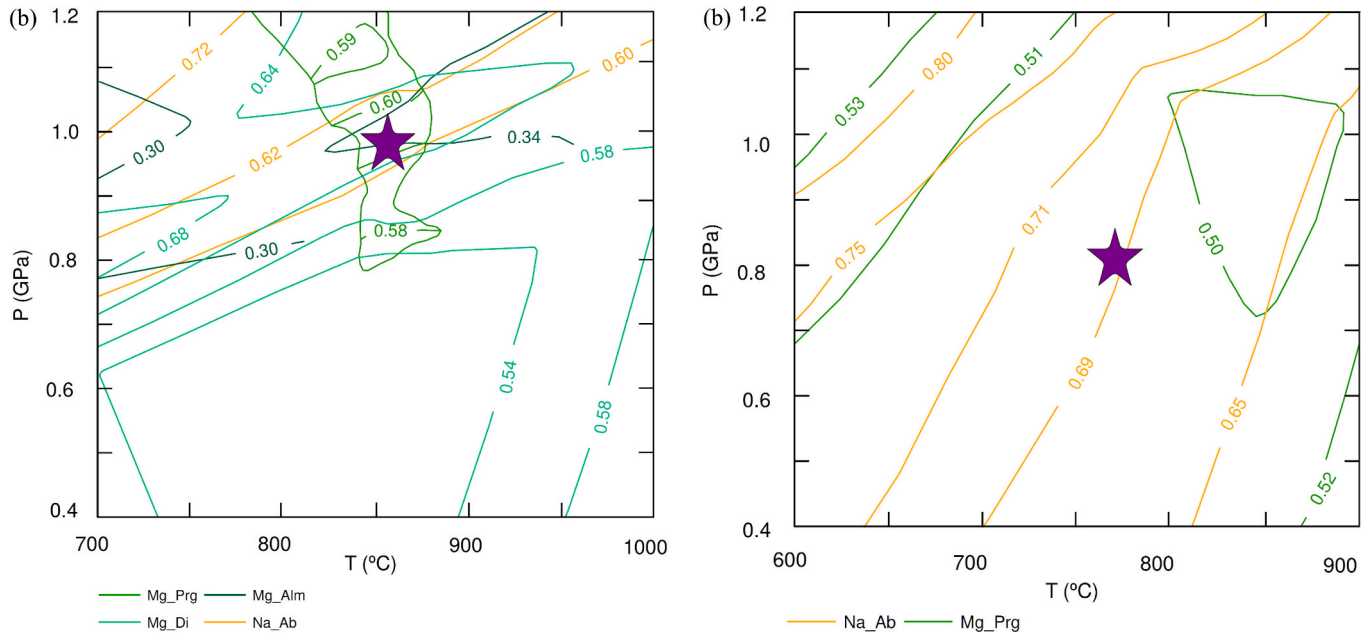

Fig. 11. a) Simplified pseudosection with compositional isopleths for the *x*Mg ratio of clinoAmp (Prg), Cpx (Di), and Grt (Alm) and *x*Na content of Pl (Ab) for the LCOx61 sample. b) Simplified pseudosection with compositional isopleths for the *x*Mg ratio of clinoAmp (Prg) and *x*Na content of Pl (Ab) for the LCOx62 sample.

mafic granulites under study have undergone incipient partial melting. Some have restite compositions, and others have partial melt compositions.

5.2. *Effect of metamorphism on element mobility*

The LOI values from studied samples are <4% (Supplementary Table 3a). These data point that post magmatic/metamorphic and alteration effects do not significantly modify their WR composition (e.g., Smith and Humphries, 1998). Only three samples display LOI values >4% (Supplementary Table 3a), but two of them have values of 4.14% (LCOx40a sample) and 4.28% (LCOx61 sample) and are not assessed. Sample LCOx42 displays a LOI value of 6.32 (Supplementary Table 3a) and indicates alteration processes, a fact that has already been observed in thin sections (Supplementary Fig. 5).

The Mg# values of LCOx69b, LCOx78, and LCOx108 samples have not been projected in Fig. 4 as they are considered outliners. LCOx69b sample have acid WR composition, and this is shown by its low Mg#

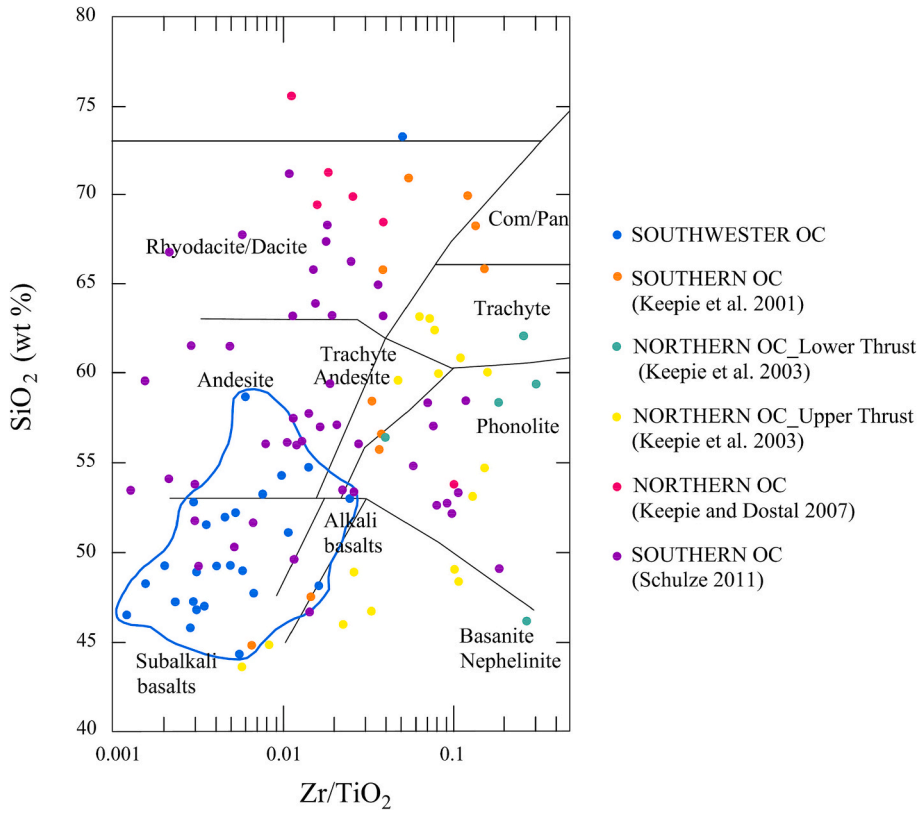

Fig. 12. Zr/TiO_2 vs. SiO_2 (wt%) diagram of Winchester and Floyd (1977). In this diagram, the studied samples from this work are projected together with the southern OC samples studied by Keppie et al. (2001) and Schulze (2011) and the northern OC samples studied by Keppie et al. (2003a) and Keppie and Dostal (2007).

=7.2 (Supplementary Table 3a). LCOx108 sample displays the highest Mg# = 65.5 (Supplementary Table 3a). This is probably related to metasomatism/hydrothermalism processes associated with the normal faults in the surrounding area (Fig. 2b). The low Mg# =25.5 of LCOx78 sample (Supplementary Table 3a) are perhaps due to the lineation structure in the vicinity of this sample (Fig. 2b).

If we look at minor and trace elements, LCOx15, LCOx49 and LCOx47 samples are enriched in all REE compared to the OIB (Fig. 5a) and have higher trace element concentrations than those from OIB (Fig. 5b). Moreover, LCOx61 sample (Fig. 5a) display much higher concentrations of light (LREE) than heavy REE (HREE). The enrichment in LREE suggests post-magmatic/metamorphic processes. These samples are grouped in pairs in the study area. LCOx15 and LCOx61 samples at the east of the center study site and LCOx49 and LCOx47 samples at the east of the southern study site (Fig. 2b). These samples are close to the sectors where structural lineations are present. *These structural lineations are not visible in the field. However, they are visible in aerial photography.

Finally, La and Ce enrichment relative to Nb, Ta and Th (Fig. 5b) is inferred to result from crustal contamination. This conclusion alignswith their negative εNd signatures (Culí et al., 2022). These results are in full agreement with those of Keppie et al. (2003a) for the mafic and intermediate granulites from northern OC:

5.3. Geotectonic setting of the mafic granulite protoliths

The studied samples are plotted in different fields depending on the geotectonic diagram. The main fields are IAB/IAT, VAB, MORB, P/*E*-MORB, WPB/WPT, CAB, and BABB (Fig. 6). The information derived from these data is consistent with the different tectonic environments related to the proto-Oaxaquia and Oaxaquia drift.

It can be observed that most of the samples from the southern center of the study site belong to divergent environments related to a) MORB or b) WP-basalts/tholeiites (Supplementary Table 8 and Fig. 2b). The emplacement of a) MORB affinity basalts supports the hypothesis that most of the mafic granulites/metabasites from the south of the study site correspond to the primitive root of the arc (therefore, probably also from the orogen). The emplacement of WP-basalts/tholeiites is in line with those rift-related basalts emplaced at 1.2–1.3 Ma studied in the northern OC by Keppie and Dostal (2007). Nevertheless, at 1.2–1.3 Ma, the supposed proto-Oaxaquia drift is in an oceanic arc/backarc geotectonic setting, not an intra-plate context. Therefore, it can be stated that G2 is mostly made up of rocks related to a divergent geotectonic setting related to the proto-Oaxaquia oceanic island arc. It is important to note that there are no reported mafic granulites outcrops such as G2 in the northern part of the OC.

Fractionated REE patterns with low HREE concentrations correspond to petrochemical features that indicate partial melting of metamorphosed and hydrated basaltic crust (e.g., Deng et al., 2019; Kunz et al., 2014). Studied samples accomplish these features (Fig. 5a). Furthermore, whether the samples studied are normalized according to CHUR or PM (Fig. 5a and b), they have similar features. Therefore, as observed in the geotectonic diagrams, the origin of most of the samples corresponds to the partial melting of metamorphosed MORB and OIB. All these conclusions are summarized in Fig. 13. Note that four WR LREE enriched patterns suggest post-magmatic metasomatism/metamorphism in two locations from the study site (Figs. 2b and 5a).

5.4. Phase equilibria modeling

Direct thermodynamic modeling by pseudosections on two samples (Grt-Amp bearing basic mafic granulite LCOx61 and Amp bearing basic mafic granulite LCOx62) has provided satisfactory results on the thermodynamic models in terms of comparison between measured and predicted (calculated) assemblages and mineral modes and compositions. The LCOx61 phase diagram model suggests that the observed

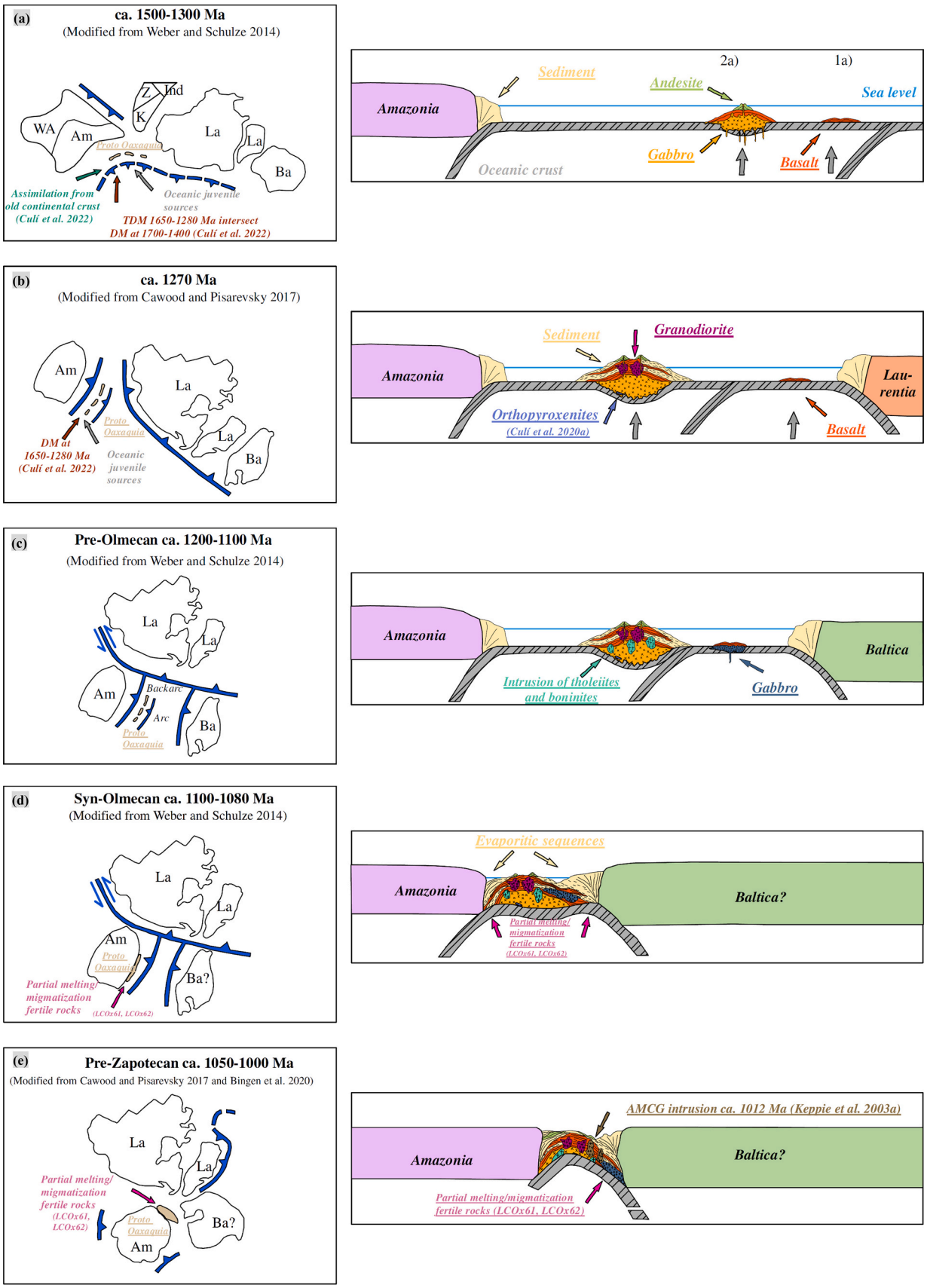

Fig. 13. Paleogeographic and tectonic model for proto-Oaxaquia/Oaxaquia, Amazonia (Am), Baltica (Ba), and Laurentia (La) during Rodinia development where the geodynamic environments are based on Weber and Schulze (2014), Cawood and Pisarevsky (2017) and Bingen et al. (2021). For details, see the text. Abbreviations: Ind = India, K=Kalahari, WA = West Africa, and Z = Zimbabwe. Drawings are not to scale.

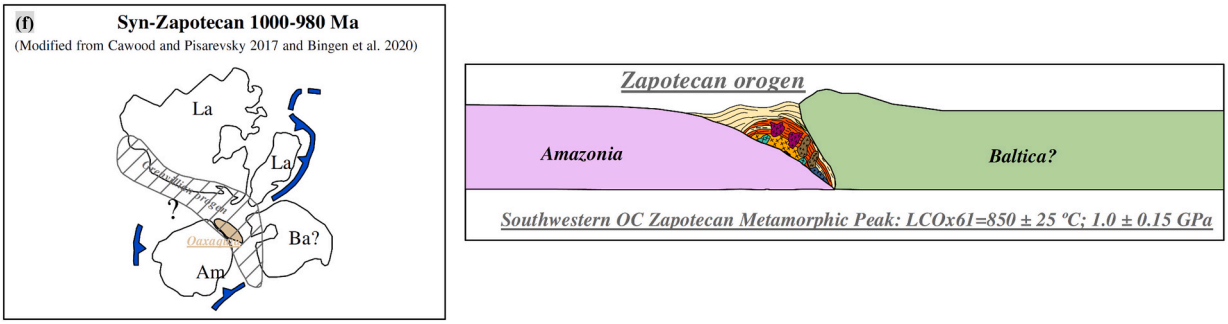

Fig. 13. (*continued*).

mineral association reached equilibrium conditions in the range of $T = 850 \pm 25$ °C and 1.0 ± 0.15 GPa, and for the LCOx62 sample, $T = 760 \pm 10$ °C and 0.8 ± 0.2 GPa (Figs. 8 and 9). These data are consistent with the classical geothermobarometry at the study site (Culí et al., 2021). The measured vs. calculated modal percentage comparisons (Fig. 10a and b) for the two modeled samples display a reasonable agreement. Also, the mineral composition isopleth diagrams (Fig. 11a and b) for the two modeled samples show a high degree of similarity with the actual mineral compositions obtained by EPMA WDS (Supplementary Tables 6a and 6b). These facts suggest that the assumed hypotheses for the construction of the model (model bulk compositions, in particular the H_2O and Fe^{3+} content) are valid, and the observed assemblages were stabilized under granulite facies P-T conditions, probably under slightly different P, T and hydration conditions. There is little evidence of mafic-derived leucosomes near the studied sample localities. Although, LCOxt61 modeled sample is located near outcrops of foliated granitic migmatites belonging to G1 (Culí et al., 2021), it is plausible that partial melting in the basic rocks from southwestern OC had been scarce. The timing of partial melting with felsic leucosomes of the southwestern OC —observed at the outcrop level and inferred from geochemical studies and modeling— is a pre-Zapotecan event (ca. 1 Ga). The thermodynamic models for mafic gneisses shown in Figs. 8 and 9 merely reflect the stabilization of granulitic assemblages by recrystallization of gabbro-dioritic intrusives without those having suffered extensive hydration and then prograde metamorphism and extensive re-melting. Metabasites melting cannot be a post-Grenvillian event since, after the Grenvillian orogeny, OC did not register any further high-grade metamorphic episode (e.g., Ortega-Gutiérrez et al., 2018).

On the other hand, prograde stage melting reactions act as a temperature buffer, so there is consensus in assuming that partial crustal melting occurs in different stages (e.g., Arkani-Hamed and Jolly, 1989) and that it is related to the fertility of the rocks (e.g., Vielzeuf et al., 1991). Any syn-Zapotecan melting event should have involved rocks that have already lost their fertility in the prograde stage, so the Zapotecan event is mainly anhydrous. Furthermore, there is no evidence of fluid infiltration during the Zapotecan orogeny, but this is beyond the scope of our study, and we hope that as knowledge of the OC evolves, this fact will be discerned.

The fundamental difference between the two modeled samples is that LCOx62 is more hydrated than LCOx61. As mentioned above, the phase equilibria diagram for the LCOx62 sample (Fig. 9) can only be obtained using an intermediate to high degree hydration (4% H_2O). The calculated modal amount of Bt is larger than the observed and should be produced during retrogradation, which is not observed in the LCOx62 sample. The presence of higher modal percentages of Amp (54%) in this sample also can suggests a later hydration episode, although, as cited in Forshaw et al. (2019), the poor estimations of Al, Ca and K arising from the present Amp solution model could be sufficient to distort the model assemblages and modes. So, for example, if more K were accepted by model Amp, this would determine less Bt in the model.

For a more detailed test of the validity of the fit of the models, a detailed comparison of various compositional parameters in the highly complex minerals has been made. The results of the detailed compositional analysis of the Amp and Cpx compositions of the modeled samples are presented in Annex I, as it is for these minerals that Green et al. (2016) establish their new *a-x* ratios.

5.5. Structure and geometry of the proto-Oaxaquia arc

Finally, Fig. 13 summarizes the most important results that can be synthesized from this study in different scenarios. The proto-Oaxaquia oceanic island arc is formed between ca. 1500–1300 Ma (Fig. 13a). The initial stage of island arc structure is the formation of an arcuate fissure through the oceanic structure. Basalt magma, fairly close to primary magma, first rises through this fissure, causing submarine volcanism (e.g., Kuno, 1968) (*1*) in Fig. 13a. Through the repeated outpouring of the magma, the oceanic crust is thickened. Then andesite magma is produced by fractionation in magma reservoirs. The extrusion of andesite magma contributes to the further thickening of the crust, coupled with the formation of more voluminous masses of gabbro left after solidifying the reservoirs. The andesitic and basaltic eruption takes place from island volcanoes projecting on this submarine ridge (e.g., Kuno, 1968) (*2*) in Fig. 13a. The proto-Oaxaquia oceanic island arc/backarc has matured at ca. 1270 Ma (convergent setting) (Fig. 13b). At this stage, lavas and pyroclastic rocks are interbedded with some sediments arising from weathering and disintegration of the rocks of the islands. The sediments may be derived from the continent where the island arc was close. As the lower crustal layer is further thickened, orogenic movement and metamorphism may occur. The lower crustal layer may be subjected to partial melting to produce granodiorite magma due to the temperature rise, which includes the upper crust (e.g., Kuno, 1968). At the same time, an oceanic arc is generated between the Amazonia and Baltica cratons, provoking the emplacement of rift-related basalts (1.2–1.3 Ga) (Keppie and Dostal, 2007). At ca. 1200–1100 Ma, proto-Oaxaquia is located within a peri-Amazonia backarc basin (Fig. 13c). At these times, there is the intrusion of tholeiitic and boninitic suites related to the initial subduction in a proto-Oaxaquia backarc basin (e.g., Yang et al., 2020). Between ca. 1100 and 1080 Ma, proto-Oaxaquia is attached to the Amazonian continental margin (Fig. 13d). At these times, the Olmecan event generated partial melting and migmatization in the older parts of proto-Oaxaquia due to the fertility of the rocks. As stated above, the time of partial melting of the southwestern OC —observed at the outcrop level (migmatites) and inferred from geochemical studies and phase equilibria modeling— is pre-Zapotecan. In this context, evaporitic sediments from the upper parts of the OC were deposited (Ortega-Gutiérrez, 1984). At ~1050 and 1000 Ma, proto-Oaxaquia sustained a subduction stage (Fig. 13e). At the same time, in the arc basin, there is the intrusion of rift-related AMCG suites (Keppie et al., 2003). At these times, partial melting and migmatization are also possible due to the fertility of subducted rocks. At 1000–980 Ma, a continent-continent collision occurred between northern Amazonia and southern Baltica craton, corresponding to the

Grenvillian (Zapotecan) orogeny (Fig. 13f). In the southwestern Oaxacan Complex, peak metamorphic conditions were 850 ± 25 °C and 1 ± 0.15 GPa as calculated for the LCOx61 sample and a later event with 760 ± 10 °C and 0.8 ± 0.2 GPa for the LCOx62 sample (Figs. 8 and 9). Finally, after ~980 Ma, the orogen cooled down. A later hydration episode is inferred through LCOx62 phase equilibria modeling (Fig. 9).

It should be noted that very recent studies (Kulakov et al., 2022) have not supported the classical Baltica-Laurentia configuration within the Rodinia supercontinent. Kulakov et al. (2022) based their study on new Bamble paleomagnetic pole reconstructions at ~1090 Ma, showing a substantial latitudinal space between the Laurentia and Baltica margins and concluding that there is no geologic nor paleomagnetic evidence for placing them next to each other. However, Kulakov et al. (2022) reconstruction of the Sveconorwegian orogen (SNO) only involves Baltica and Laurentia, overlooking the possible role of Amazonia in a three continental plates collisional scenario. Also, an Andean accretionary model was suggested for the SNO as an alternative to the canonical collisional model generally accepted for the entire worldwide Grenvillian orogen (see Weller et al., 2021 for a recent review). The tectonometamorphic register of the Zapotecan orogeny (1000–980 Ma) of the OC is more in line with a continent-continent encounter because: 1) it recorded ultra HT metamorphic conditions (Culí et al., 2020; Ramírez-Salazar et al., 2022); 2) other than Proto-Oaxaquia, which may have been an intra oceanic arc that probably collided with Amazonia ~1100 Ma ago, there is no evidence for further accretion of other arcs, nor ophiolitic complexes or accretionary sedimentary successions; 3) Proterozoic massif anorthosite AMCG complexes have not been recorded in oceanic accretionary systems, but they constitute the hallmarks of the Grenville belt (e.g., Corrigan and Hanmer, 1997) including Oaxaquia; and 4) after the Zapotecan orogeny, the OC remained part of an exposed craton for almost 500 Ma (Ortega-Gutiérrez et al., 1995). Hence, here we still assume a true collisional setting between Baltica and Amazonia to explain the nature and age of the OC and correlative Grenvillian units of the northwestern Andes (e.g., Ibañez-Mejía et al., 2011).

6. Conclusions

The southwestern OC intermediate/basic mafic granulites (metabasites) have a main mineral association corresponding to Pl + Cpx + Bt/Amp ± Grt ± Opx ± Fsp (perthitic) ± Qz. Their plutonic protoliths are mainly gabbro and gabbro-diorite, and volcanic protoliths mainly correspond to basalt and basaltic andesite, linked to the island arc or arc magmatism at convergent plate margins of proto-Oaxaquia.

The partly evolved Mg# (<50) and the concomitant decrease in Cr and Ni from studied metabasites suggest that these metamorphic rocks have experienced a marked pre-emplacement fractionation of Ol and Px, whereas only rocks with relatively evolved compositions have been intruded.

Following geotectonic diagrams, most of the basic mafic granulites from the south of the study area (G2 group) correspond to the primitive root of the arc and probably of the orogen, related to the proto-Oaxacan island arc.

The southwestern OC metabasites constitute an assemblage apart from the rest of the Oaxacan Complex metabasites due to their Ti enrichment and SiO_2 depletion related to post-magmatic/metamorphic processes.

The origin of most of the samples corresponds to the partial melting of metamorphosed MORB and OIB emplaced in a divergent geotectonic environment according to fractionated REE patterns. Ba/Th ratios from orthogneisses under study have undergone incipient partial melting. The time of partial melting of the southwestern OC metabasites —which has been observed at the outcrop level (migmatites) and inferred from geochemical studies and modeling— is a pre-Zapotecan (Grenvillian) event (ca. 1 Ga).

Direct thermodynamic modeling by pseudosections from the Grt-Amp bearing basic mafic granulite (LCOx61 sample) phase diagram model suggests that the observed mineral phase association reached equilibrium conditions in the range of $T = 850 \pm 25$ °C and 1.0 ± 0.15 GPa, and for the Amp-bearing basic mafic granulite (LCOx62 sample), $T = 760 \pm 10$ °C and 0.8 ± 0.20 GPa. A later hydration episode is deduced from the phase equilibria diagram for the LCOx62 sample, which can only be obtained using an intermediate to high degree hydration (4% H_2O) and the presence of higher modal percentages of Amp. Based on the data presented in this work and the existing literature, the Green et al. (2016) *a-x* relations are very good at predicting Na in the M4 position for amphiboles but underestimate Ca in M4 and K in the A position and overestimate tetrahedral site cations Al^{IV}, Al^{T} and Al^{IV} according to Forshaw et al. (2019).

Declaration of Competing Interest

The authors declare that they have no known competing financial interests or personal relationships that could have appeared to influence the work reported in this paper.

Acknowledgments

This work corresponds to an area studied by the first author in her Ph.D. thesis. This project has been financed by CONACYT grant 240226 and DGAPA-UNAM grant IN111917 to J. Solé. We thank Spanish Ministerio de Economía, Industria y Competitividad through Projects: PID2019-109018RB-I00 and 2015-66335-C2-2-R. We thank the following people: Teresa Pi Puig, Marc Campeny from Museu de Ciències Naturals de Barcelona, Xavier Llovet from Serveis Cientifico Tècnics de la Universitat de Barcelona, and Marco Antonio Argaez for fieldwork. We thank Dr. Dave Waters and an anonymous reviewer for their comments that improved the manuscript.

Appendix A. Supplementary data

Supplementary data to this article can be found online at https://doi.org/10.1016/j.lithos.2023.107239.

References

Andersson, U.B., Ghebreab, W., Teklay, M., 2006. Crustal evolution and metamorphism in east-Central Eritrea, south-east Arabian-Nubian Shield. J. Am. Earth Sci. 44, 45–65.
Arkani-Hamed, J., Jolly, W.T., 1989. Generation of Archean tonalites. Geology 17, 307–310.
Bingen, B., Viola, G., Möller, C., Auwera, J.V., Laurent, A., Yi, K., 2021. The Sveconorweigian orogeny. Gondwana Res. 90, 273–313.
Cawood, P.A., Pisarevsky, S.A., 2017. Laurentia-Baltica-Amazonia relations during Rodinia assembly. Precambrian Res. 292, 386–397.
Corrigan, D., Hanmer, S., 1997. Anorthosite and related granitoids in the Grenville orogen: a product of convective thinning of the lithosphere? Geology 25, 61–64.
Cortesogno, L., Gaggero, L., Zanetti, A., 2000. Rare earth and trace elements in igneous and high-temperature metamorphic minerals of oceanic gabbro (MARK area, Mid-Atlantic Ridge). Contrib. Mineral. Petrol. 139, 373–393.
Culí, L., 2020. Petrología, Geoquímica, Termobarometría, Pseudosecciones metamórficas y Geocronología de la porción centro-sur del Complejo Oaxaqueño, Oaxaca, Mexico. PhD Thesis. Universidad Nacional Autónoma de México, p. 217.
Culí, L., Solé, J., Ortega-Gutiérrez, F., 2020. Metamorphic evolution of Proterozoic ultramafic rocks from the Oaxacan complex (Oaxaca State, southern Mexico): Tectonic implications. In: Martens, U., Molina, R. (Eds.), Southern and Central Mexico: Basement Framework, Tectonic Evolution, and Provenance of Mesozoic-Cenozoic Basins. GSA Special Volume, Chapter, p. 5.
Culí, L., Solé, J., Campeny, M., Oalmann, J.A.G., 2021. High-Temperature Metamorphic Garnets from Grenvillian Granulites of Southwestern Oaxacan complex (southern Mexico): Petrology, Geochemistry, Geothermobarometry, and Tectonic Implications. Minerals 11, 805.
Culí, L., Solé, J., Schaaf, P., Solís-Pichardo, G., Oalmann, J., Campeny, M., 2022. Sm-Nd isotope whole rock and garnet from the southwestern Grenvillian Oaxacan complex, Mexico: a review of garnet closure temperature and structural implications. J. S. Am. Earth Sci. 119, 103967.
De Capitani, C., Petrakakis, K., 2010. The computation of equilibrium assemblage diagrams with Theriak/Domino software. Am. Mineral. 95, 1006–1016.
Deng, J., Yang, X., Qi, H., Zhang, Z.F., Mastoi, A.S., Al Emil, G.B., Sun, W., 2019. Early cretaceous adakite from the Atlas porphyry Cu-Au deposit in Cebu Island, Central Philippines: partial melting of subducted oceanic crust. Ore Geol. Rev. 110, 102937.

Diener, J., Powell, R., 2012. Revised activity-composition models for clinopyroxene and amphibole. J. Metamorph. Geol. 30, 1312–1420.
Fitz-Bravo, C., Castillo-Reynoso, J.E., 2010. Carta Geológico-Minera. Ejutla de Crespo E14D67 (Oaxaca). Servicio Geológico Mexicano (SGM), scale 1, 50000.
Forshaw, J.B., Waters, D.J., Pattison, D.R., Palin, R.M., Gopon, P., 2019. A comparison of observed and thermodynamically predicted phase equilibria and mineral compositions in mafic granulites. J. Metamorph. Geol. 37, 153–179.
Gillis, R.J., Gehrels, G.E., Ruiz, J., Flores, L.A., 2005. Detrital zircon provenance of Cambrian-Ordovician and Carboniferous strata of the Oaxaca terrane, southern Mexico. Sediment. Geol. 182, 87–100.
Green, E.C.R., Holland, T.J.B., Powell, R., 2007. An order-disorder model for omphacitic pyroxenes in the system jadeite-diopside-hedenbergite-acmite, with applications to eclogitic rocks. Am. Mineral. 92, 1181–1189.
Green, E.C.R., White, R.W., Diener, J.F.A., Powell, R., Holland, T.J.B., Palin, R.M., 2016. Activity-composition relations for the calculation of partial melting equilibria in metabasic rocks. J. Metamorph. Geol. 34, 845–869.
Holland, T., Powell, R., 2003. Activity–composition relations for phases in petrological calculations: an asymmetric multicomponent formulation. Contrib. Mineral. Petrol. 145, 492–501.
Holland, T., Powell, R., 2011. An improved and extended internally consistent thermodynamic dataset for phases of petrological interest, involving a new equation at state for solids. J. Metamorph. Geol. 29, 333–383.
Holland, T., Green, E.C.R., Powell, R., 2018. Melting at peridotites through to granites: a simple thermodynamic model in the system KNCFMASHTOCr. J. Petrol. 59, 881–900.
Ibañez-Mejía, M., Ruiz, J., Valencia, V.A., Vardona, A., Gehrels, G.E., Mora, A.R., 2011. The Putumayo Orogen of Amazonia and its implications for Rodinia reconstructions: New U-Pb geochronological insights into the Proterozoic tectonic evolution of northwestern South America. Precambrian Res. 191, 58–77.
Jorgensen, T.R.C., Tinkham, D.K., Lesher, C.M., 2019. Low-P and high-T metamorphism of basalts: insights from the Sudbury impact melt sheet aureole and thermodynamic modelling. J. Metamorph. Geol. 37, 271–313.
Kelemen, P.B., Hanghøj, K., Greene, A.R., 2014. One view of the geochemistry of subduction-related Magmatic Arcs, with an emphasis on primitive andesite and lower crust. In: Holland, T., Heinrich, D., Turekian, K.K. (Eds.), Treatise on Geochemistry. Elsevier, Amsterdam, pp. 749–806.
Keppie, J.D., Dostal, J., 2007. Rift-related basalts in the 1.2-1.3 Ga granulites of the northern Oaxacan complex, southern Mexico: evidence of a rift arc on the northern western margin of Amazonia. Proc. Geol. Assoc. 118, 63–74.
Keppie, J.D., Dostal, J., Ortega-Gutiérrez, F., Lopez, R., 2001. A Grenvillian arc on the margin of Amazonia: evidence from the Southern Oaxacan complex, Southern Mexico. Precambrian Res. 112, 165–181.
Keppie, J.D., Dostal, J., Cameron, K.L., Solari, A., Ortega-Gutiérrez, F., Lopez, R., 2003. Geochronology and geochemistry of Grenvillian igneous suites in the northern Oaxacan complex, southern Mexico: tectonic implications. Precambrian Res. 120, 365–389.
Kulakov, E.V., Slagstard, T., Ganerod, M., Torsvik, T.H., 2022. Paleomagnetism and 40Ar/39Ar geochronology of Meso-Neoproterozoic rocks from Southwest Norway. Implications for magnetic remanence ages and the paleogeography of Baltica in a Rodinia supercontinent context. Precambrian Res. 397, 106786.
Kuno, H., 1968. Origin of andesite and its bearing on the island arc structure. Bull. Volcanol. 32, 141–176.
Kunz, B.E., Johnson, T.E., White, R.W., Redler, C., 2014. Partial melting of metabasic rocks in Val Strona di Omegna, Ivrea Zone, northern Italy. Lithos 190, 1–12.
Le Maitre, R.W., 2002. Igneous Rocks: A classification and glossary of terms. In: Streckeisen, A., Zanettin, B., Le Bas, M.J., Bonin, B., Bateman, P., Bellieni, A., Dudke, S., Efremova, J., Keller, J., Maneyre, P.A., Dudek, R., Schmid, H., Sorensen, H., Woolley, A.R. (Eds.), Cambridge University Press, p. 236.
Leake, B.E., 1964. The Chemical Distinction between Ortho- and Para-amphibolites. J. Petrol. 5, 238–254.
Li, Z.X., Bogdanova, S.V., Collins, A.S., Davidson, A., Waele, B.D., Ernst, R.E., Fitzsimons, I.C.W., Fuck, R.A., Gladkochub, D.P., Jacobs, J., Karstrom, K.E., Lu, S., Natapov, L.M., Pease, V., Pisarevsky, S.A., Thrane, K., Vernilovsky, V., 2008. Assembly, configuration, and breakup history of Rodinia: a synthesis. Precambrian Res. 160, 179–210.
Lozano, R., Bernal, J.P., 2005. Characterization of a new set of eight geochemical reference materials for XRF major and trace element analysis. Revista Mexicana de Ciencias Geologicas 22, 3.
Meschede, M., 1986. A method of discriminating between different types of mid-ocean ridge basalts and continental tholeiites with the Nb-Zr-Y diagram. Chem. Geol. 56, 207–218.
Middlemost, E.A.K., 1994. Naming materials in the magma/igneous rocks system. Earth Sci. Rev. 37, 215–224.
Naslund, H.R., 2007. Norm Calculation. Geol. Sci. SUNY-Binghamton, Binghamton, NY, p. 13902.
Ortega-Gutiérrez, F., 1984. Evidence of Precambiran evaporites in the Oaxacan granulite complex of southern Mexico. Precambrian Res. 23, 377–393.
Ortega-Gutiérrez, F., Ruiz, J., Centero-García, E., 1995. Oaxaquia, a Proterozoic microcontinent accreted to North America during the late Paleozoic. Geology 23, 11327-1130.
Ortega-Gutiérrez, F., Elías-Herrera, M., Morán-Zentero, D.J., Solari, L., Weber, B., Luna-González, L., 2018. The Pre-Mesozoic metamorphic basement of Mexico, 1.5 billion years of crustal evolution. Earth-Sci. Rev. 183, 2–37.
Palin, R.M., White, R.W., Green, E.C.R., 2016. Partial melting of metabasic rocks and the generation of tonalitic-trondhjemitic-granodioritic (TTG) crust in the Archean: Constrains from phase equilibrium modelling. Precambrian Res. 287, 73–90.
Pearce, J.A., Norry, M.J., 1979. Petrogenetic implications of Ti, Zr, Y, and Nb variations in volcanic rocks. Contrib. Mineral. Petrol. 69, 33–47.
Powell, R., Downes, J., 1990. Garnet porphyroblast-bearing leucosomes in metapelites: mechanisms, phase diagrams, and an example from Broken Hill, Australia. In: Ashworth, J.R., Brown, M. (Eds.), High-temperature Metamorphism and Crustal Anatexis. The Mineralogical Society Series, 2. Springer, Dordrecht.
Ramírez-Salazar, A., Almazán-López, M., Colás, V., Ortega-Gutiérrez, F., 2022. Multi-thermobarometry and microstructures reveal ultra-high temperature metamorphism in the Grenvillian Oaxacan complex, Southern Mexico. Int. Geol. Rev. 6, 1–23.
Renner, J., Evans, B., Hirth, G., 2000. In the rheologically critical melt fraction. Earth Planet. Sci. Lett. 181, 585–594.
Rollinson, H., Pease, V., 2021. Using Geochemical Data to Understand Geological Processes. Cambridge University Press.
Rudnick, R.L., 1992. Restites, Eu Anomalies and the Lower Continental Crust: Geochemical et Cosmochimica Acta, 56, pp. 963–970.
Rudnick, R.L., Gao, S., 2003. Composition of the continental crust. In: Holland, H.D., Turekeian, K.K. (Eds.), Treatise on Geochemistry. The crust Chp.3. Elsevier, Oxford, pp. 1–64.
Rudnick, R.L., Gao, S., 2014. Composition of the continental crust. In: Holland, H.D., Turekeian, K.K. (Eds.), Treatise on Geochemistry. The Crust Chp.4. Elsevier, Oxford, pp. 1–51.
Saccani, E., 2015. A new method of discriminating different types of post-Archean ophiolitic basalts and their tectonic significance using Th-Nb and Ce-Dy-Yb systematics. Geosci. Front. 6, 481–501.
Salters, V.J., Stracke, A., 2004. Composition of the depleted mantle. Geochem. Geophys. Geosyst. 5.
Schulze, C., 2011. Petrología y Geoquímica de las Rocas del Área de Pluma Hidalgo, Oaxaca e Implicaciones tectónicas para el Proterozoico de Oaxaquia. PhD. Thesis. Universidad Nacional Autónoma de México, p. 369.
Servicio Geológico Mexicano (SGM), 2000. Carta Geológico-Minera. Zaachila E1412 (Oaxaca). scale 1, 250000.
Shchepetilnikova, V., Solé, J., Solari, L.A., 2015. Chronological and chemical zircon study of some pegmatite dikes and lenses from the Central Part (Ayoquezco–Ejutla) of the Oaxacan complex, Southern Mexico. Revista Mexicana de Ciencias Geológicas 32, 123–143.
Smith, S.E., Humphries, S.E., 1998. Geochemistry of basaltic rocks from the TAG hydrothermal mount (26°08'N), Mid-Atlantic Ridge. In: Herzig, P.M., Humphries, S. E., Miller, D.J., Zierenberg, R.A. (Eds.), Proceedings of the Ocean Drilling Program, Scientific Results 158. Texas A & M University Press, College Station, pp. 213–229.
Solari, L.A., Keppie, J.D., Ortega-Gutiérrez, F., Cameron, K.L., Lopez, R., Hames, W.E., 2003. 990 and 1100 Ma Grenvillian tectonothermal event in the northern Oaxacan complex, southern Mexico: Roots of an orogeny. Tectonophysics 365, 257–282.
Stüwe, K., 1997. Effective bulk composition changes due to cooling: a model predicting complexities in retrograde reaction textures. Contrib. Mineral. Petrol. 129, 43–52.
Sun, S.S., McDonough, W.F., 1989. Chemical and isotopic systematics of ocean basalts. Implications for mantle compositions and processes. In: Saunders, A.D., Norry, M.J. (Eds.), Magmatism in Ocean Basins. Geological Society Special Publications, London, pp. 313–345.
Treloar, P.J., 1987. The Cr-minerals of Outokumpu. Their chemistry and significance. J. Petrol. 867, 867–886.
Uribe-Luna, J., Pérez-Reynoso, X., 2012. Carta Geológico-Minera. San Baltazar Loxicha E14D87 (Oaxaca). In: Servicio Geológico Mexicano (SGM), scale 1:50000.
Vielzeuf, D., Clemens, J.D., Pin, C., Moinet, E., 1991. Granites, granulites and crustal differentiation. In: Vielzeuf, D., Vidal, P. (Eds.), Granulites and Crustal Evolution. NATO ASI Series, Springer, Dordrecht, pp. 59–85.
Weber, B., Schulze, C., 2014. Early Mesoproterozoic (>1.4 Ga) ages from granulite basement inliers of SE Mexico and their implications on the Oaxaquia concept. Evidence from U-Pb and Lu-Hf isotopes on zircons. Revista Mexicana de Ciencias Geológicas 31, 377–394.
Weller, O.M., Mottram, C.M., St-Onge, M.R., Möller, C., Strachan, R., Rivers, T., Copley, A., 2021. The metamorphic and magmatic record of collisional orogens. Nat. Rev. Earth Environ. 2, 781–799.
White, R.W., Powell, R., Holland, T.J.B., Worley, B., 2000. The effect of TiO_2 and Fe_2O_3 on metapelitic assemblages at greenschist and amphibole facies conditions: mineral equilibria calculations in the system K_2O-FeO-MgO-Al_2O_3-SiO_2-H_2O-TiO_2-Fe_2O_3. J. Metamorph. Geol. 18, 497–511.
White, R.W., Powell, R., Clarke, G.L., 2002. The interpretation of reaction textures in Fe-rich metapelitic granulites of the Musgrave Block, Central Australia: constrains from mineral equilibria calculations in the system K_2O-FeO-MgO-Al_2O_3-SiO_2-H_2O-TiO_2-Fe_2O_3. J. Metamorph. Petrol. 20, 41–55.
White, R.W., Powell, R., Holland, T.J.B., Johnson, T.E., Green, E.C.R., 2014a. New mineral activity-composition relations for thermodynamic calculations in metapelitic systems. J. Metamorph. Geol. 32, 261–286.
White, R.W., Powell, R., Johnson, T.E., 2014b. The effect of Mn on mineral stability in metapelites revised: a new a-x relations for manganese-bearing minerals. J. Metamorph. Geol. 32, 809–828.
Whitney, D.L., Evans, B.W., 2010. Abbreviations for names of rock-forming minerals. Am. Mineral. 95, 185–187.
Winchester, J.A., Floyd, P.A., 1977. Geochemical discrimination of different magma series and their differentiation products using immobile elements. Chem. Geol. 20, 325–343.
Yang, G., Li, Y., Tong, L., Wang, Z., Si, G., 2020. An early Cambrian plume-induced subduction initiation event with the Jungggar Ocean: Insights from ophiolitic mélanges, arc magmatism, and metamorphic rocks. Gondwana Res. 88, 45–66.